International Journal of Thermal Sciences 111 (2017) 256–273

Contents lists available at ScienceDirect

International Journal of Thermal Sciences

journal homepage: www.elsevier.com/locate/ijts

Fluid-structure interaction study of natural convection heat transfer over a flexible oscillating fin in a square cavity

Mohammad Ghalambaz [a, *], Esmail Jamesahar [a], Muneer A. Ismael [b], Ali J. Chamkha [c, d]

[a] Department of Mechanical Engineering, Dezful Branch, Islamic Azad University, Dezful, Iran
[b] Mechanical Engineering Department, Engineering College, University of Basrah, Basrah, Iraq
[c] Mechanical Engineering Department, Prince Mohammad Bin Fahd University, Al-Khobar, 31952, Saudi Arabia
[d] Prince Sultan Endowment for Energy and Environment, Prince Mohammad Bin Fahd University, Al-Khobar, 31952, Saudi Arabia

ARTICLE INFO

Article history:
Received 16 March 2016
Received in revised form
6 August 2016
Accepted 4 September 2016

Keywords:
Oscillating fin
Cavity
Natural convection
Fluid-structure interaction

ABSTRACT

The material of this study is a numerical formulation of a fluid-structure interaction represented by an oscillating elastic fin attached to a hot vertical wall of a square cavity. The cavity is filled with air, $Pr = 0.7$, and differentially heated while the horizontal walls are kept adiabatic. The finite element Galerkin method with the aid of the Arbitrary Lagrangian-Eulerian (ALE) procedure is used in the numerical analysis. The elastic fin undergoing an excitation and is subjected to buoyancy forces. The ranges of the studied parameters are the Rayleigh number $Ra = 10^4$–10^7, fin length $L = 0.1$–0.4, oscillating amplitude $A = 0.001$–0.1, oscillating period $\tau = 0.01$–1, thermal conductivity ratio (fin to fluid) $k_r = 1$–1000, and the non-dimensional Young's modulus $E = 10^8$-10^{13}. The results show that increasing the non-dimensional amplitude the oscillating fin can significantly enhance the Nusselt number. The non-dimensional periods about $\tau \approx 0.1$ and higher shows better enhancement compared to lower periods. A fin length of 0.2 can be considered as the best length for heat transfer enhancement and compatible with various oscillating amplitudes.

1. Introduction

The enormous development of electronic technology has become more pronounced in many engineering, industrial, and environmental applications. This development did not exist without an accompanied progress in heat rejection (cooling) methods. Enhancement of natural convection has been and will continue to be pivotal in improving the performance of the cooling mechanisms of electronics contained in enclosures. During the last two decades, there has been a developing efficient mechanism for enhancing the natural convection by exciting the entire enclosure or its boundaries using an external mechanical or an electrical force. Hence, this mechanism is unrestricted by the electrical or thermal properties of the fluid. The analysis of such problem is classified as a moving boundary problem, which is encountered in many engineering applications and in nature as well. Cooling fan induced vibration in electronic devices, biological micro-scale experiments, mixing and sterling devices, and heat exchangers are examples of these applications. These problems are classified as fluid-structure interaction (FSI) which is often used for unsteady flow interacting in two ways manner between the fluid and solid boundaries. The effects of vertical vibration and gravity on the induced convection inside enclosure were simulated by Fu and Sheih [1,2]. Kimoto and Ishidi [3] investigated the vibration effects on the natural convection heat transfer in a square enclosure. Fu et al. [4] reported a remarkable increase in heat transfer associated with laminar forced convection in a parallel-plate channel including an oscillating block. Florio and Harnoy [5] studied the enhancement of natural convection cooling of discrete heat source in a vertical channel using a vibrating plate. Convection in porous media undergoing mechanical vibration is reported by Razi et al. [6]. Chung and Vafai [7] investigated the vibrational and buoyancy induced convection in a vertical porous channel with an open-ended top and a vibrating left wall. Cheng et al. [8] proposed a novel approach to enhance the convective heat transfer in heat exchanger by using the flow induced vibration instead of strictly avoiding it.

However, in devices cooling strategy, imposing vibration to the

* Corresponding author.
E-mail addresses: m.ghalambaz@iaud.ac.ir (M. Ghalambaz), behravan.jam@gmail.com (E. Jamesahar), muneerismael@yahoo.com, muneer.ismael@uobasrah.edu.iq (M.A. Ismael), achamkha@pmu.edu.sa (A.J. Chamkha).

http://dx.doi.org/10.1016/j.ijthermalsci.2016.09.001
1290-0729/

Nomenclature

A	amplitude of the oscillating fin
b	fin thickness
$\boldsymbol{d}_s$	displacement vector
E	Young's modulus
$\boldsymbol{F}_v$	body force vector
$\boldsymbol{g}$	gravitational acceleration vector
H	cavity length
k	Thermal conductivity
L	Fin length
Nu	Nusselt Number
P	Pressure
Pr	Prandtl number
Ra	thermal Rayleigh number
Re	Reynolds number in Ref. [26]
t	time
T	temperature
TR	period of the fin's oscillation/convection time in Ref. [28]
$\boldsymbol{u}$	velocity vector
W	work
x,y	Cartesian coordinates

Greek symbols

α	thermal diffusivity
β	thermal expansion coefficient
λ	Frequency of the oscillation
ν	kinematic viscosity
ρ	density
σ	stress tensor
τ	period of oscillation
υ	Poisson's ratio

Subscripts

c	cold
f	fluid
fixed	a *fixed fin without oscillation*
h	hot
local	local value
oscillating	an *oscillating fin*
P	partition
r	the property ratio of the solid to the fluid
s	solid

Superscripts

*	dimensional parameters

heated surface/enclosure can seriously reduce the reliability and stability of the electronic device. Therefore, the increasing demands of heat removing have resulted in very effective mechanisms using passive or active enhancing techniques represented by thin fins attached to heat generating surfaces. The passive technique can be referred to flexible thin fin(s) placed in a flow undergoing a convective heat transfer. Ben-Nakhi and Chamkha [9,10] investigated the effect of the presence of a fixed thin fin on the heat transfer in a cavity. They [10] analyzed the effect of fin lengths equal to 20, 35 and 50% of the hot wall. They found that the effect of the fin length on the heat transfer rate in the cavity acted in an unordered way. The authors discussed this unordered way as being due to fact that the addition of a fin to an enclosure simultaneously restrained natural convection flow in the cavity but increased the heat transfer from the surface due to the enhanced conduction mechanism in the fin.

Turek and Hron [11] developed a self-sustained oscillation in 2D laminar channel flow basing on an elastic plate attached to the lee side of a rigid cylinder. Another method namely, sharp-interface Cartesian grid, was proven capable of simulating thin flexible structures as documented by Vigmostad et al. [12]. Nevertheless, the later attentions were focused on the Turek and Horn simulation procedures [13–17] including adaptive finite element approximation [13], comparison of segregated versus monolithic solvers [14], dealing with large deformation effects [15,16], and induced movements due to oscillation of the flow [17].

Khanafer et al. [18] studied the effects of the flow conditions and the geometric variation of the microcantilever's bluff body on the microcantilever detection capabilities within a fluidic cell. Their main result was that the introduction of a random noise in the fluidic cell which caused the microcantilever to oscillate in a harmonic mode at low velocity. Soti et al. [19] demonstrated numerically a large-scale flow-induced deformation as an effective passive heat transfer enhancement technique. They investigated the thermal augmentation as well as quantified the flow-induced deformation of an elastic thin plate attached to lee side of a rigid cylinder in a heated channel laminar flow.

The active augmentation technique utilizes the reversed piezoelectric effect that is either gluing the base of the fin on an oscillating specific element or bonding a piezoelectric patch on the surface of a thin fin. This technique is known as piezoelectric fan. The low consumed power, less noise, compact with light weight, and significantly heat dissipative have led to important contribution of piezoelectric fan in the development of powerful electronic devices. Toda and Osaka [20] reported that the temperature of a TV receiver could be dropped from 66 to 49 °C by 14 mW only provided to fan actuated using piezoelectric polymer PVF2. Yoo et al. [21] investigated several vibrating metal plates forming piezoelectric cooling fans. They found that the phosphor bronze vibrating plate is the most effective design. They correlated the physical properties and the vibrating plate dimensions in a useful equation that determines the resonance frequency.

Aciklican et al. [22] proved experimentally that the piezoelectric fans can provide subsistence cooling in hot spots where the rotary fan is inactive such as in some situations in a laptop and a personal computer. While in smaller devices (cellular phones for example) the piezoelectric fan could be wholly relied on. They reported 100% enhancement in the local heat transfer coefficient. Liu et al. [23] found experimentally that the fin tip plays a major role in inducing a jet-like air stream which in turn can augment the heat transfer. Kimber et al. [24] developed correlations to predict the thermal performance of a piezoelectric fan. These correlations are based on dimensionless parameters including the piezoelectric fan dimensions and the dynamic characteristics namely, and frequency of fin vibration and the amplitude. Ma and Li [25] obviated the insufficient cooling ability of piezoelectric fan for LEDs by using a dual-sided multiple fans arrangement with piezoelectric actuator ("D-MEPA"). Their results presented that the dimensionless heat convection number could be enhanced from 2.82 with 0.22 Watts power input to 3.92 with 0.2 Watts power input for a single piezoelectric fan and dual-sided multi fans, respectively. Sheu et al. [26] manufactured and tested nine piezoelectric fins subjected to various bonding and piezoelectric patches. They reported that the heat transfer augmentation can be 64% at 5 Watt only. Their study

showed that the bonding glue played a significant role on the fin tip displacement, where those of higher Young's modulus gave larger fan tip displacement.

In contrast with piezoelectric fan technology, the fin-based oscillating technique has received less investigation attention. The reason may be attributed to the belief that this process may catch with the problem accompanying the method of vibrating the heated body/enclosure. For instance, the work of Fu and Yung [27] proposed the concept of inducing externally thin fins by an oscillation exciter. The fins were swinging back and forth in a flowing fluid. In general, their results showed that the swinging fins could contract and disturb the velocity and thermal boundary layers, hence, attaining a considerable heat transfer enhancement. The swinging fin speed influenced the performance of the instantaneous circulation zones.

However, the survey concerning the vibrating thin fin inside enclosures has shown that this topic is limited to the co-researchers Shi and Khodadadi [28,29]. Their specific case was a lid-driven square cavity with a hot upper wall being lid to the right and the other walls were fixed and kept isothermal at a cold temperature. A horizontally oscillating thin fin extruded from the right vertical wall was used. Their analysis ignored the natural convection, and they used the finite volume method as a numerical appliance. Their interesting results have shown that the time taken for the mean Nusselt number to reach its peak values is dependent on the distance between the fin tip and the respective wall while is independent on the fin oscillating frequency.

In a very recent study, Jamesahar et al. [30] have studied the natural convection heat transfer in a cavity diagonally divided into two triangular partitions using a flexible partition membrane using the ALE formulation. They addressed the effect of the flow induced by natural convective heat transfer on the large deformation of the membrane due to fluid-structure interaction. They have also investigated the effect of the induced changes in the membrane shape on the heat transfer in the cavity.

Now, it is clear from the above literature survey that the problem of enhancement of heat transfer inside cavities by an oscillating thin fin has received very little investigation effort. Moreover, an oscillating fan-like fin inside cavities has never been investigated, according to the best authors' survey. Thus, the vehicle of the present study is the numerical analysis of the convective heat transfer in a square differentially heated cavity with an oscillating elastic thin fin placed at the mid height of the vertical hot wall. This case is classified as a moving mesh problem, and hence, the Arbitrary Lagrangian- Eulerian (ALE) method is intended to be followed.

2. Mathematical model

The problem under consideration is shown schematically in Fig. 1. It is a two-dimensional, differentially heated, square cavity with a side length H. The horizontal walls are adiabatic. The right vertical wall is cooled isothermally and kept at a temperature T^*_c, while the right vertical wall is heated isothermally and kept at a temperature T^*_h. A thermally-conductive elastic thin fin with a length L^* and a thickness b^* is attached in a cantilever form on the mid height of the hot vertical wall. The free end of the elastic fin oscillates sinusoidally as per the following equation:

$$y^* = A^* \sin(\frac{2\pi t^*}{\tau^*}) \tag{1}$$

where y^* is the vertical position of the free end of the fin, t^* is the time, A^* is the oscillation amplitude and τ^* is the oscillation period. Accordingly, the oscillation frequency can be defined as $\lambda^* = 1/\tau^*$. The fluid flow inside the cavity is considered laminar, incompressible, and Newtonian. The fluid thermo-physical properties are independent of the temperature variation and the Boussinesq approximation for density is applicable. The Joule-heating effect is neglected. The governing equations for the geometrically nonlinear elasto-dynamic structural displacement and energy of the fin can be written as:

$$\rho_s \frac{d^2 \mathrm{d}_s^*}{dt^{*2}} - \nabla\sigma^* = \mathrm{F}_v^* \tag{2}$$

$$\frac{\partial T^*}{\partial t^*} = \alpha_s \nabla^2 T^* \tag{3}$$

The governing equations of conservation of mass, momentum and energy in the Arbitrary Lagrangian–Eulerian (ALE) formulation are written as:

$$\nabla \mathrm{u}^* = 0 \tag{4}$$

$$\frac{\partial \mathrm{u}^*}{\partial t^*} + (\mathrm{u}^* - \mathrm{w}^*)\cdot\nabla \mathrm{u}^* = -\frac{1}{\rho_f}\nabla P^* + {}^*\nu_f \nabla^2 \mathrm{u}^* + \beta \mathrm{g}_y \left(T^* - T_c^*\right) \tag{5}$$

$$\frac{\partial T^*}{\partial t^*} + (\mathrm{u}^* - \mathrm{w}^*)\cdot\nabla T^* = \alpha_f \nabla^2 T^* \tag{6}$$

where σ^* is the stress tensor, $\boldsymbol{d_s^*}$ is the solid displacement vector, $\boldsymbol{F_v^*}$ is the applied body force, $\boldsymbol{u}^*$ is the fluid velocity vector, $\boldsymbol{w}^*$ is the moving coordinate velocity, P^* is the fluid pressure and T^* is the fluid/solid temperature. The densities of the solid and fluid are respectively denoted by ρ_s and ρ_f. Here, α_s and α_f represent the thermal diffusivity of the solid and fluid, respectively. ν_f is the kinematic viscosity of the fluid, $\boldsymbol{g_y}$ is the gravitational acceleration, and β is volumetric thermal expansion coefficient.

Considering the fin as linearly elastic, and taking into account the nonlinear geometry effects, the stress tensor σ is written as

$$\sigma = \mathrm{J}^{-1}\mathrm{FSF}^{\mathrm{T}} \tag{7}$$

where $\mathrm{F} = (\mathrm{I} + \nabla \mathrm{d}_s^*)$ and $\boldsymbol{J} = \det(\boldsymbol{F})$. The second Piola-Kirchhoff stress tensor $\boldsymbol{S}$ is related to strains ($\boldsymbol{\varepsilon}$) as

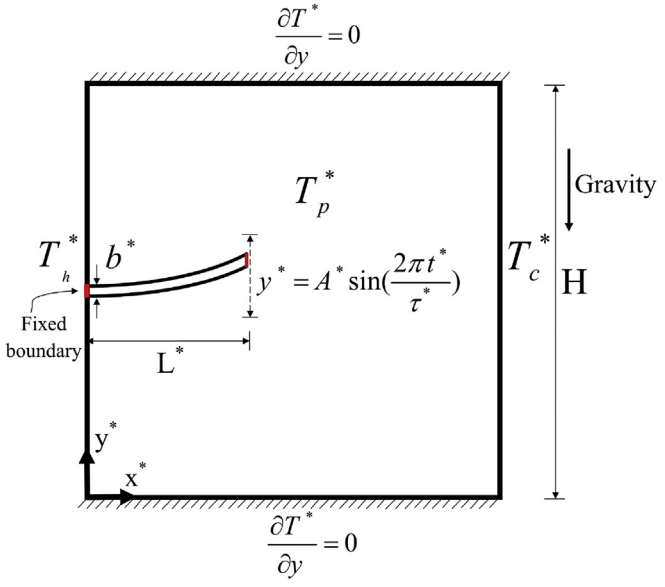

Fig. 1. A schematic representation of the cavity with an oscillating fin.

$$S = C : (\varepsilon) \quad \text{with} \quad \varepsilon = \frac{1}{2}\left(\nabla d_s^* + \nabla d_s^{*T} + \nabla d_s^{*T}\nabla d_s^*\right) \tag{8}$$

where $C = C(E^*,\nu)$. In Eq. (1), $\boldsymbol{F}_{\boldsymbol{v}}^*$ is the gravitational force per unit volume, which is written as $\rho_s \boldsymbol{g}_{\boldsymbol{y}}$. The boundary conditions for the fluid-solid interaction at the fin surfaces are continuity of kinematic forces and dynamic movements. Considering the regular no-slip boundary condition for the fluid at the solid interface results in:

$$\frac{\partial d_s^*}{\partial t^*} = u^* \quad \text{and} \quad \sigma^* \cdot n = -P^* + \mu_f \nabla u^* \tag{9}$$

For the energy equation, the energy balance at the interface of solid-fluid:

$$k_f \frac{\partial T^*}{\partial n} = k_s \frac{\partial T^*}{\partial n} \tag{10}$$

The fin under consideration is assumed to be clamped with $\partial d_s^*/\partial t^* = 0$. The pressure constraint is a condition applied at the top left corner of the cavity such as:

$$P^* = 0 \tag{11}$$

For the initial conditions, it is assumed that the cavity connected to the hot and cold walls are respectively at uniform temperatures of T^*_h and T^*_c, and the fluid is quiescent (i.e. $\boldsymbol{u}^* = 0$). Now, the following non-dimensional parameters are used to non-dimensionalize the governing equations:

$$d_s = \frac{d_s^*}{H}, \quad \sigma = \frac{\sigma^*}{E^*}, \quad t = \frac{t^*\alpha_f}{H^2}, \quad (x,y) = \frac{(x^*,y^*)}{H}, \quad (A,L,b) = \frac{(A^*,L^*,b^*)}{H}, \quad \tau = \frac{\tau^*\alpha_f}{H^2} \tag{12a}$$

$$(u,v) = \frac{(u^*,v^*)H}{\alpha_f}, \quad w = \frac{w^*H}{\alpha_f}, \quad P = \frac{H^2}{\rho_f\alpha_f^2}P^*, \quad T = \frac{T^* - T_c^*}{T_h^* - T_c^*}. \tag{12b}$$

The governing Equations (2)–(6) are written in the following non-dimensional form:

$$\frac{1}{\rho_R}\frac{d^2 d_s}{dt^2} - E\nabla\sigma = EF_v \tag{13}$$

$$\frac{\partial T}{\partial t} = \alpha_r \nabla^2 T \tag{14}$$

$$\nabla u = 0 \tag{15}$$

$$\frac{\partial u}{\partial t} + (u - w)\cdot\nabla u = -\nabla P + Pr\nabla^2 u + Pr\cdot RaT\,\hat{e}_j \tag{16}$$

$$\frac{\partial T}{\partial t} + (u - w)\cdot\nabla T = \nabla^2 T \tag{17}$$

by using the following non-dimensional parameters:

$$Ra = \frac{g_y\beta\left(T_h^* - T_c^*\right)H^3}{\upsilon_f\alpha_f}, \; Pr = \frac{\upsilon_f}{\alpha_f}, \; E = \frac{E^*H^2}{\rho_f\alpha_f^2}, \; F_v = \frac{\left(\rho_f - \rho_s\right)Hg_y}{E^*}, \; \rho_r = \frac{\rho_f}{\rho_s}, \; \alpha_r = \frac{\alpha_s}{\alpha_f} \tag{18}$$

In the above equation, Ra and Pr are the Rayleigh and Prandtl numbers, respectively. E, α_r, ρ_r and $\boldsymbol{F}_{\boldsymbol{v}}$ are the flexibility and body force parameters, thermal diffusivity ratio, the density ratio parameter and the body force parameters. It should be noted that $\boldsymbol{F}_{\boldsymbol{v}}$ which denotes the non-dimensional body force is positive when the density of the fin is lower than the density of the fluid inside the cavity. In this case the body force is positive and tends to move the fin upward. Most of practical fins are stiff, and hence, the shape of the fin is free of strong influence of the buoyancy force. Thus, in the present study, the influence of the buoyancy force on the fin is neglected (i.e. $\boldsymbol{F}_{\boldsymbol{v}} = 0$) for convenience. Here, it is useful to introduce the stream function ψ as $u = \partial\psi/\partial y, v = -\partial\psi/\partial x$.

The boundary conditions are written in the following non-dimensional forms:

$$T = 0 \text{ at the cold right wall, } T = 1 \text{ at the hot left wall, } \partial T/\partial n = 0 \text{ at the horizontal walls} \tag{19}$$

$$\left(\frac{\partial T}{\partial n}\right) = k_r\left(\frac{\partial T}{\partial n}\right) \quad \text{for the fin} \tag{20}$$

where $k_r = k_s/k_f$.

The solid-fluid interaction boundary conditions are also written as:

$$\frac{\partial d_s}{\partial t} = u \text{ and } E\sigma\cdot n = -P + Pr\nabla u \tag{21}$$

The non-dimensional initial temperature at the fluid and the fin is $T = 0.5$. The non-dimensional initial velocity is $\boldsymbol{u} = 0$. For the pressure point constraint, the following non-dimensional pressure constraint is also considered:

$$P = 0 \tag{22}$$

The non-dimensional tip displacement of the fin is also obtained as:

$$y = A\sin\left(\frac{2\pi\, t}{\tau}\right) \tag{23}$$

where A is the non-dimensional oscillation amplitude (introduced in Eq. (12a)), and τ is the non-dimensional period (introduced in Eq. (12a)).

In the present study, the parameter of interest is the Nusselt number, which shows the heat transfer from the wall. The local Nusselt number along at the hot wall is written as:

$$Nu = h\cdot Y\big/k_f \quad \text{at} \quad x = 0 \tag{24}$$

where h is the local convective heat transfer coefficient at the wall and k_f is the thermal conductivity of the fluid. The conductive heat transfer from the hot wall can be divided into two parts: the conduction heat transfer into the fluid and the conduction heat transfer through the basis of the fin, which can be written as:

$$\begin{cases} q_{cond} = -k_f \dfrac{\partial T^*}{\partial x^*} & \text{at interface of the wall and fluid} \\ q_{cond} = -k_s \dfrac{\partial T^*}{\partial x^*} & \text{at interface of wall and solid (the basis of the fin)} \end{cases} \tag{25}$$

By invoking the non-dimensional parameters, Eq. (25) results in:

$$\begin{cases} Nu_{local,f}(t) = -\dfrac{\partial T(t)}{\partial x} & \text{at interface of wall and fluid} \\ Nu_{local,s}(t) = -k_r \dfrac{\partial T(t)}{\partial x} & \text{at interface of wall and solid} \end{cases} \tag{26}$$

where $k_r = k_s/k_f$. The average Nusselt number at the basis of the fin can be introduced as:

$$Nu_s(t) = \int_{s_1}^{s_2} Nu_{local,s}(t)dy \quad \text{where} : \begin{cases} s_1 = \dfrac{1}{2} - \dfrac{b}{2} \\ s_2 = \dfrac{1}{2} + \dfrac{b}{2} \end{cases} \tag{27}$$

The average Nusselt number at the hot wall is also introduced as:

$$Nu(t) = \int_0^{s_1} Nu_{local,f}(t)dy + \int_{s_1}^{s_2} Nu_{local,s}(t)dy + \int_{s_2}^{H} Nu_{local,f}(t)dy \tag{28}$$

The average Nusselt number over time can be evaluated as:

$$Nu = \int_1^{1+5\tau} Nu(t)dt \tag{29}$$

where the non-dimensional time of $t \approx 1$ is a very large time scale in which the flow and heat transfer in the presence of the fin oscillations have reached to a semi-steady situation. Then, the time averaging for the Nusselt number is commenced over five periods of oscillation ($t = [1, 1+5\tau]$). The enhancement/deterioration parameter describing the magnitude of heat transfer changes can be introduced as:

$$NNR = \frac{Nu_{oscillating} - Nu_{fixed}}{Nu_{fixed}} \times 100 \tag{30}$$

where the subscripts "*oscillating*" and "*fixed*" denote the time average Nusselt number for a fin when oscillates and the time average Nusselt number for a fin when it is fixed, respectively. Indeed, NNR denotes the thermal enhancement of using an oscillating fin over a fixed fin.

The required work (W^*) for oscillation of the fin can be evaluated using the dot product of the reaction force ($\boldsymbol{F}^*$) at the tip of the fin and the fin tip displacement ($\boldsymbol{d}_s^*$) as $W^* = \boldsymbol{F}^* . \boldsymbol{d}_s^*$, in which the reaction force is the vector product of the tension and the cross section of the fin tip as $\boldsymbol{F}^* = \boldsymbol{\sigma}^* \times b^*$. Therefore, the non-dimensional work ($W = W^*/(E^* H^2)$) required for the oscillation of the fin can be obtained as:

$$W = (\sigma b) \cdot d_s \tag{31}$$

3. Numerical method and validations

The governing Equations (13)–(17) with the prescribed boundary conditions, that are non-linear and interdependent, are to be solved numerically. Due to the vibration of the fin through a fluid, it is more accurate to consider that the fin nodes (solid) along with neighboring finer fluid nodes pursuing a time moving boundary problem. An efficient numerical technique which deals with such problem is the Arbitrary Lagrangian-Eulerian (ALE) method. This method consorts the facility of moving boundary domain (provided by the Lagrangian method), holding a fixed domain (provided by the Eulerian method), and the moving procedure. This method is well discussed in Hirt et al. [31], Hughes et al. [32], Donea et al. [33], and Kuhl et al. [34]. Hence, the nonlinear governing Equations (13)–(17) are transformed into the weak form and discretized using the Galerkin finite element method (see Ref. [35]). The computational domain is meshed by applying non-uniform triangular grids. The calculations are stopped at any time step for which the error is less than 10^{-7}.

3.1. Grid independency test

Firstly, it is necessary to ensure that the results obtained are independent of the number of mesh elements, and therefore, grid independency tests are performed. For this purpose, the dimensionless temperature at the point (x = 0.15, y = 0.8) is examined with dimensionless time at both the initial and steady states for four mesh sizes (see Table 1). The results are presented for $Ra = 10^6$, $Pr = 0.7$, $A = 0.05$ and $k_r = 10$ in Figs. 2 and 3. Fig. 2 denotes the results for the case of the high oscillation period of $\tau = 1.0$, and Fig. 3 depicts the results for the very low oscillation period of $\tau = 0.01$. These figures confirm that the mesh of case 3 (27131domain elements and 1022 boundary elements) is the most suitable mesh from the accuracy and processing time points of view. Hence, the mesh of case 3 is adopted throughout the present study and it is shown in Fig. 4.

3.2. Comparisons with other published work

As a further validation, the present code is adopted to solve several previously solved problems for comparison purpose. As a first validation, we made a comparison with the steady state results of natural convection in a simple rigid square cavity available in literature. In this case, the regular cavity without a fin is considered while the top and bottom walls of the cavity are insulated and the sidewalls are differentially heated. The steady state results in the present study are obtained using a transient solution of the problem after elapsing of long times when the solution reaches to its steady state situation. The comparison between the results of the present study and the results reported by Deng and Tang [36], Anandalakshmi and Basak [37], Vahl Davis [38], Shi and Khodadadi [39], Sathiyamoorthy and Chamkha [40], and Nag et al. [41] is shown in Table 2. As seen, there is excellent agreement with the results of the present study and the previous studies.

The second validation is a steady state conjugate natural convection in a square cavity. For this purpose, the results of present

Table 1
Grid details in every grid used in grid check.

Cases	Domain elements	Boundary elements
Case 1	4797	250
Case 2	7918	307
Case 3	27131	1022
Case 4	31915	1022

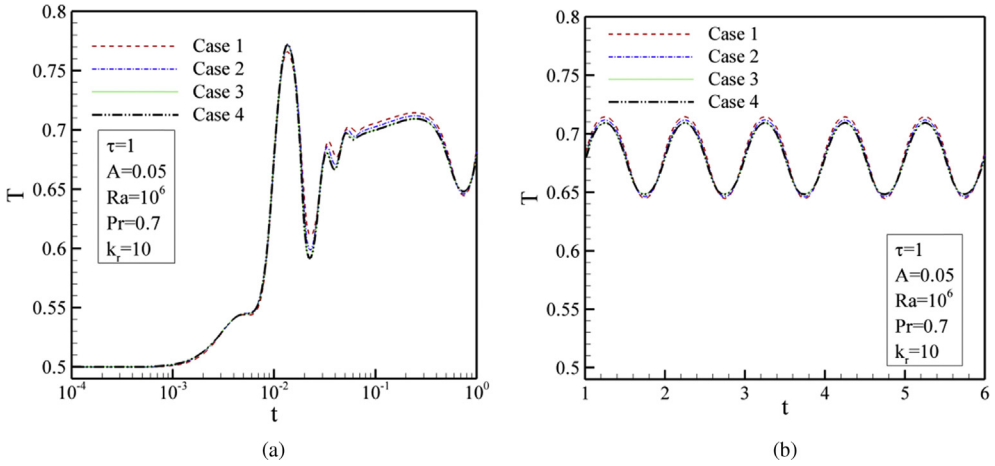

Fig. 2. Time series for the temperature at point A ($x = 0.15, y = 0.8$) calculated in different grids in logarithmic view for $\tau = 1$; (a) initial states (b) normal view for semi-steady state (b).

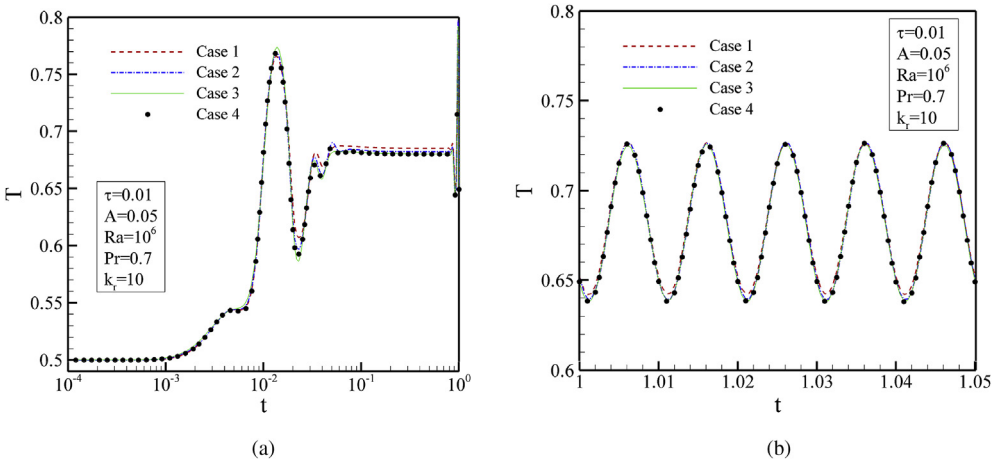

Fig. 3. Time series for the temperature at point A ($x = 0.15, y = 0.8$) calculated in different grids in logarithmic view for $\tau = 0.01$; (a) initial states (b) normal view for semi-steady state (b).

study are compared with those reported by Kaminski and Prakash [42]. The top and bottom cavity walls are thermally insulated and the sidewalls are differentially heated. Kaminski and Prakash [42] considered a finite thickness and a finite thermal conductivity for one of the side walls of the cavity while the other three walls were taken to be of zero thickness. The dimensionless parameter of the thermal conductivity ratio (k_r) was defined as the ratio of the solid to the fluid thermal conductivities (k_s/k_f). The comparison results for the average Nusselt number for various Grashof numbers ($Gr = Ra \times Pr$) are shown in Table 3. As seen, there is excellent agreement between the results of the present code and the results reported by Ref. [42].

A third comparison is performed with the results reported by Ben-Nakhi and Chamkha [43] for conjugate natural convection in a square cavity with an inclined thin fin at the hot wall. The fin is attached to the left hot thin wall while the other walls are thick with finite thermal conductivity. The left wall is assumed to be heated while the external sides of other three walls are assumed to be cold. The comparison between the values of streamlines obtained in the present study, using the finite element method, and the results reported by Ref. [43] which were obtained using the finite volume method, is shown in Table 4 which shows excellent agreement as well.

As an unsteady case, we have evaluated the correctness and accuracy of our results with the results obtained by Xu et al. [44]. They assumed a very thin and thermal conductive solid partition inside a cavity and hence, neglected the effect of conductive heat transfer in the partition. This validation is represented by comparing the dimensionless temperature reported by Ref. [44] and the temperature in the current study at the specified point (0.0083, 0.375). It is necessary to mention that the definition of the dimensionless time in our investigation and Xu et al. [44] is different. The dimensionless time defined by Xu et al. [44] is $t = t\alpha Ra^{1/2}/L^2$. The results for different grid sizes are plotted in Fig. 5. This figure indicates that the time history of the present study and the results of Xu et al. [44] are in very good agreement.

The reliability of the present code is further validated by resolving the case of vibrating fin attached to an enclosure wall which is reported by Shi and Khodadadi [28]. They [28] utilized the finite-volume-method using Patankar's SIMPLE algorithm to handle the moving fin. In the study of Shi and Khodadadi [28], the bottom and side walls of the cavity are subject to constant cold temperature T^*_c while the moving top wall is hot with a constant temperature T^*_h. A horizontal moving fin with the initial length of $L = 0.1$H is attached to the middle of the right vertical wall. The oscillating amplitude and frequency of the fin are $A = 0.05$ and

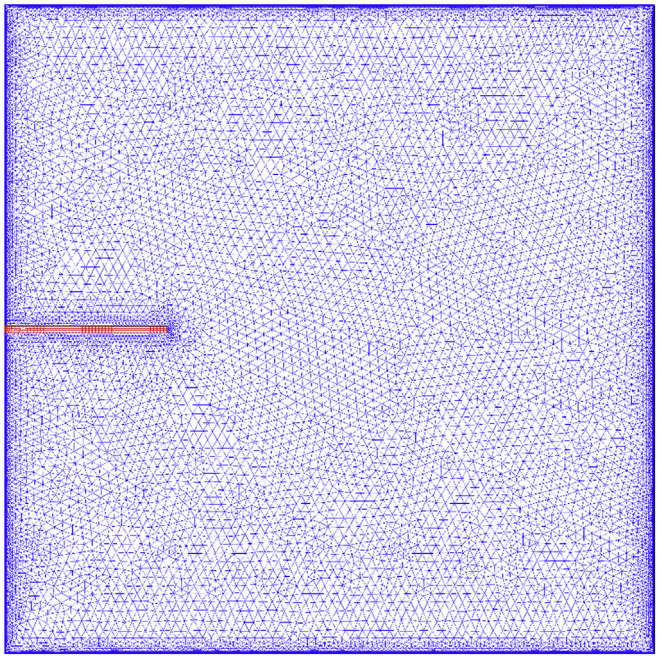

Fig. 4. The utilized grid, Case 3.

Table 2
Comparing reported Nusselt number on hot wall at present study with other for square cavity (Pr = 0.7) in various Rayleigh number.

Ra	10^3	10^4	10^5	10^6
Deng and Tang [36]	1.1180	2.2540	4.5570	–
Anandalakshmi and Basak [37]	1.1179	2.2482	4.5640	–
Vahl Davis [38]	–	2.2430	4.5190	8.8800
Shi and Khodadadi [39]	–	2.2470	4.5320	8.8930
Sathiyamoorthy and Chamkha [40]	–	2.2530	4.5840	8.9210
Nag et al. [41]	–	2.2400	4.5100	8.8200
Present study	1.1178	2.2450	4.5237	8.8663

Table 3
Comparing the average Nusselt number reported in Kaminski and Prakash [42] and present study when $Pr = 0.7$

Gr	k_s/k_f	Kaminski and Prakash [42]	Present study
10^3	1	0.87	0.87
	5	1.02	1.02
	10	1.04	1.04
	∞	1.06	1.06
10^5	1	2.08	2.08
	5	3.42	3.40
	10	3.72	3.70
	∞	4.08	4.06
10^6	1	2.87	2.86
	5	5.89	5.85
	10	6.81	6.80
	∞	7.99	7.99
10^7	1	3.53	3.51
	5	9.08	9.02
	10	11.39	11.30
	∞	15.09	15.08

λ = 1, respectively. In this case, we calculate the transient mean Nusselt number along the bottom wall while the top wall is lid-driven to the right for Re = 100 and TR = 1 where TR is defined in Ref. [28] as the period of the fin's oscillation/convection time. The results are listed in Table 5 which reveals very acceptable agreement with [28]. Globally, accreditation can be given now to the results collected by the present numerical code.

Table 4
Comparing the valves of $\Delta\psi_{ext}$ reported in Ben-Nakhi and Chamkha [43] and evaluated results in the present study when $Pr = 0.707$, $Ra = 10^5$, ε (fin inclination) = 105° and L_f (fin length) = 0.35.

k_s/k_f	Ben-Nakhi and Chamkha [43]	Present study
1	11.38	11.30
5	13.10	13.10
10	13.30	13.20
∞	13.34	13.30

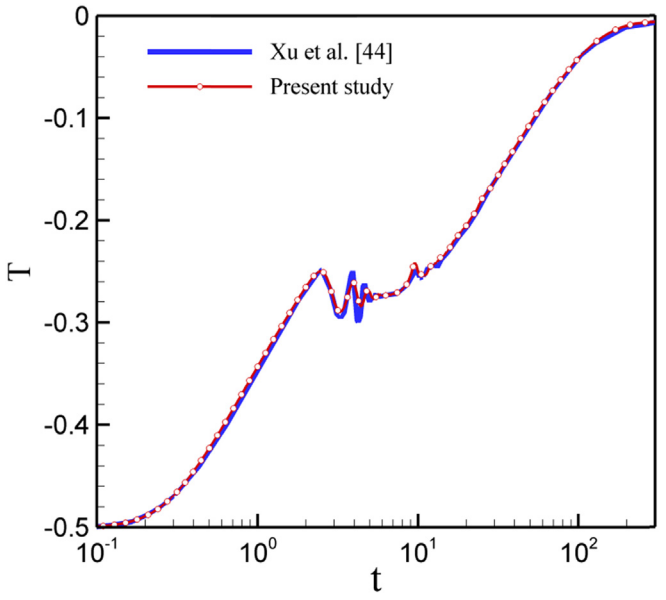

Fig. 5. Comparison with Xu et al. [44] in the case of square cavity divided into two parts by a rigid divider.

4. Results and discussion

The reported results are considered for air (Pr = 0.7), and the effects of pertinent parameters on the fluid flow, stress tensor, and thermal field are studied within the following ranges: Rayleigh number $Ra = 10^4$–10^6, Young's modulus $E = 10^8$-10^{13}, non-dimensional fin length $L = 0.2$–0.4, non-dimensional amplitude $A = 0.001$–0.1, non-dimensional period $\tau = 0.01$–1, and thermal conductivity ratio $k_r = 1$–1000. In addition, as the fin domain is very thin and small compared to the fluid domain, and the transient temperature changes in the fin in the semi-steady state condition are low, the transient heat transfer effects (the heat storage effects) in the fin are not important. Hence, it is assumed that $\alpha_r = k_r$ for convenience.

Table 5
Comparison of transient mean Nusselt number along the bottom wall [28] case at various non-dimensional time steps when $Re = 100$ and $TR = 1$.

t	Shi and khodadadi [28]	Present study
0	0.5061	0.5028
1.5	0.5104	0.5069
4.2	0.4930	0.4930
8	0.4708	0.4799
10	0.4793	0.4782
14	0.4785	0.4771
18	0.4783	0.4775

4.1. Effect of oscillation on the field variables

The effect of oscillation of the fin on the changes in the shape of the mesh, streamlines and isotherms is studied in Figs. 6–8. A close view to the fin and the mesh surrounding it is made for each one of these nine points and presented in Fig. 6. The views of this figure show the fin deformation along with movement of mesh with dimensionless time when $E = 10^{11}$, $\tau = 1$, $A = 0.1$, $Ra = 10^6$, $Pr = 0.7$ and $k_r = 10$.

Fig. 7 shows the transient evolution of the streamlines for $Ra = 10^6$, $\tau = 0.5$, and $A = 0.1$. Initially, at $t = 10^{-4}$, very weak streamlines arranged in multicellular fashion are seen. Two cells, under and above the fin, close to the hot wall, and one cell close to the cold vertical wall are observed. At $t = 10^{-3}$ (Fig. 7b), the streamlines are strengthened and indicate the onset of the flow towards the cavity core. When t evolves to $10^{-2.38}$ (Fig. 7c), strengthened streamlines manifest a clear triple-eye circulation. In this figure, the fin oscillation effect can be characterized by the intensified and stagnant flows under and above the fin, respectively. This can be attributed to the fact that when the fin is oscillating upward, a vacuum is generated under the fin surface. This vacuum is assisted by the buoyancy effect resulting in an intensified flow. Beyond $10^{-2.38}$, rapid strengthened streamlines with a main circulation vortex pouch the under-fin cell, while a secondary cell still appears above the fin (Fig. 7 (d)–(e)). When t goes to $10^{-1.64}$ and further to 10^{-1} (Fig. 7 (f)–(i)), the fin free end reaches its maximum upper deflection and the main vortex breaks up into a double–eye fashion. At t = 1, (Fig. 7k) the fin recovers its nominal horizontal shape and the secondary vortex appears again. After a longer time is elapsed, $t = 1.375$ (Fig. 7k), the fin reaches its maximum lower deflection with the absence of the secondary cell and mostly a stratification behavior of streamlines, hence the dominance of natural convection can be recognized. Fig. 8 shows the transient evolution of the isotherms for the same parameters of Fig. 6. At initial times, t = 10^{-4}-10^{-3}, a pure conduction is presented as shown in Fig. 8 (a)-(b). Little disturbed isotherms evolve close to the oscillating fin and at the lower right corner of the cavity at t = $10^{-2.38}$ (Fig. 8c). The isothermal substantial zone occupying most of the cavity, which is associated in the dimensionless times ($t = 10^{-4}, 10^{-2.38}$) is disturbed slightly at $t = 10^{-2.14}$-10^{-2} (Fig. 8 (d)-(e)). For $t > 10^{-2}$, the isotherms are aligned in a mostly horizontal behavior with noticeable perturbation in the zone surrounding the oscillating fin. Dense isotherms close to the hot wall and especially under fin are observed. These dense isotherms, which form a thermal boundary layer, contract and extend vertically depending on the fin tip position.

4.2. The effect of the fluid-structure interaction

By assuming a fin with a very high value of Young's modulus, the effect of the presence of the fluid on the changes in the shape of the fin diminishes. In this case, it seems that the fin moves in a vacuum. However, when the Young's modulus of the fin is low, the presence of the fluid and interaction between the fluid and structure would affect the shape of the fin accordingly.

Figs. 9–12 show the effect of the non-dimensional Young's modulus on the shape of the fin at different time snaps when $\tau = 0.1$, $A = 0.05$, $Ra = 10^6$ and $Pr = 0.7$ for a period of the motion of the fin after the flow in the cavity reaches a semi-steady solution ($t \approx 1$). The time snaps corresponding for labels of (a)-(e) in these figure are reported in Table 6. Table 6 also shows the maximum non-dimensional stress values of σ_{max} corresponding to Figs. 9–12. The results in this table are multiplied by 10^4, and then they have been reported for convenience. Careful analysis of the results reveals that the maximum non-dimensional value of tension occurs at the basis of the fin. The minimum non-dimensional value of

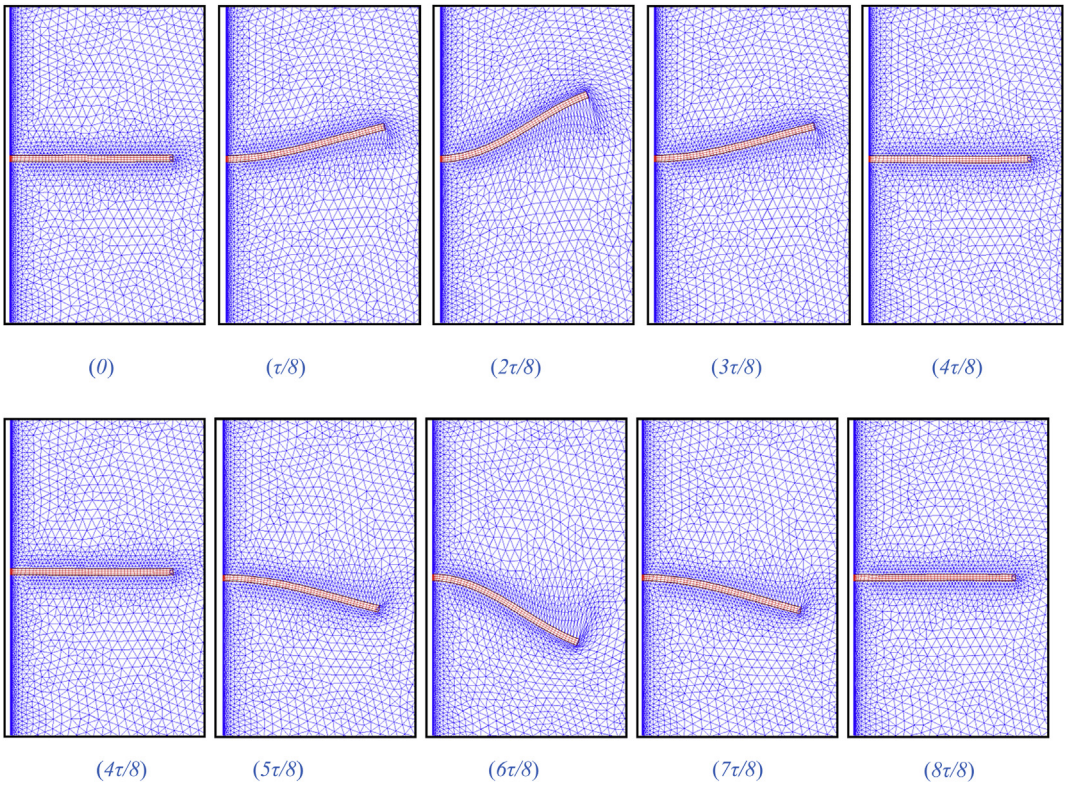

Fig. 6. Snap shots of the moving mesh surrounding the oscillating fin for different fin positions commencing from $t = 1.0$.

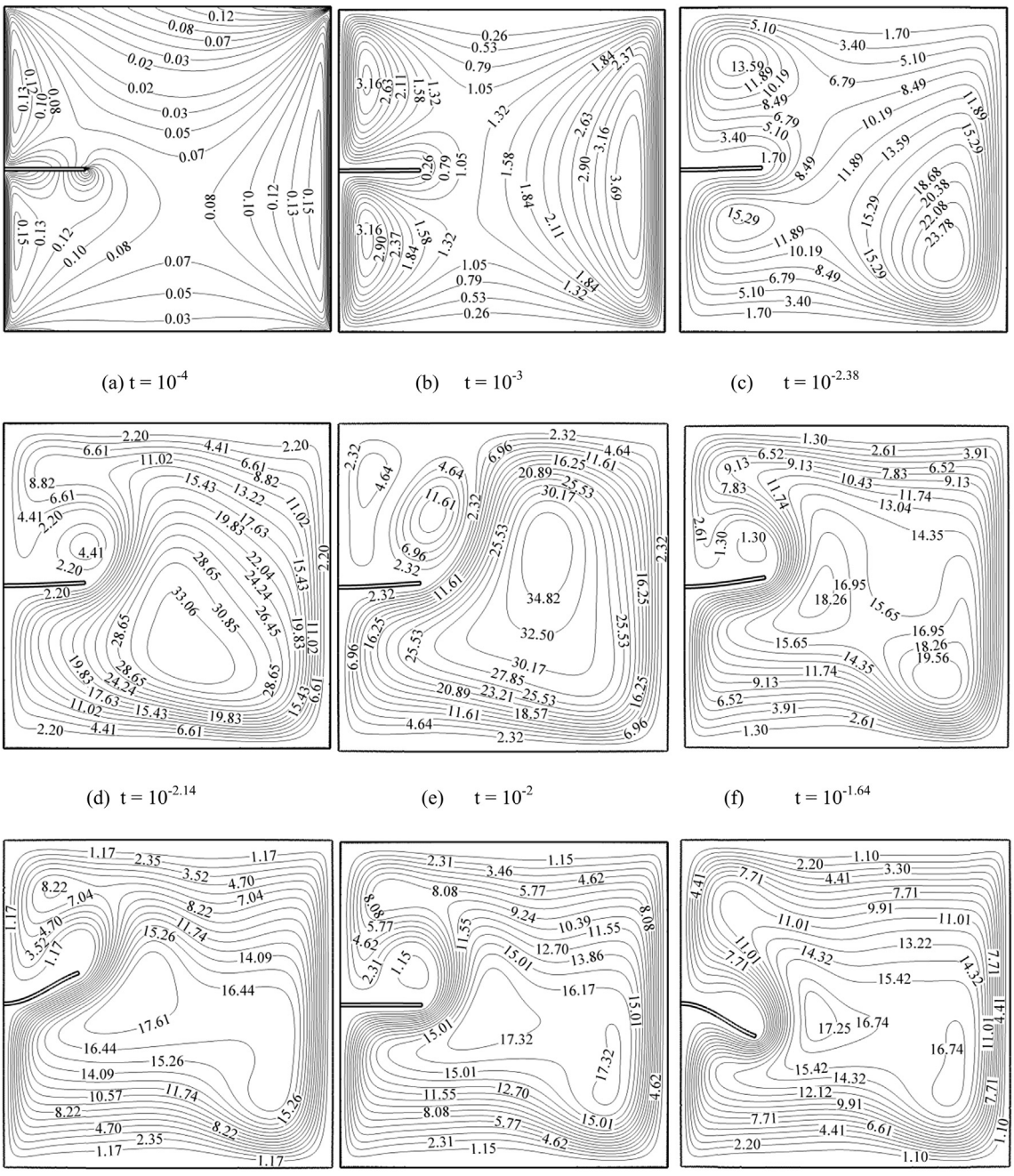

Fig. 7. Streamlines for various dimensionless times at $E = 10^{11}$, $\tau = 0.5$, $A = 0.1$, $k_r = 10$, $Ra = 10^6$, $Pr = 0.7$.

tension occurs at the tip of the fin. Based on the introduced boundary conditions, the tip of the fin should strictly follow the oscillating motion defined by Eq. (23). Therefore, in all of the figures, Figs. 9–12 and at the similar snap shots, the position of the tip of the fin is the same. The shape of the fin is under the influence of the change in the position of the tip of the fin (as a boundary condition) and the interaction with the fluid flow as a distributed force acting on the surfaces of the fin.

A comparison between the shapes of the fin in Figs. 11 and 12 at similar time steps demonstrates that when the non-dimensional Young's modulus is high, e.g. $E = 10^{12}$ and $E = 10^{13}$, the shape of the fin is not under the influence of the presence of the fluid. Indeed, these figures represent the shape of the fin in a vacuum. In contrast, when the non-dimensional Young's modulus is comparatively low, e.g. $E = 10^8$ and $E = 10^9$ as shown in Figs. 9 and 10, the shape of the beam is under significant influence of the interaction with the fluid. Indeed, in Fig. 9 which is reported for the case of $E = 10^8$, the upward flow of the fluid does not let the fin move downward due to the constraint oscillating motion of the fin tip. Hence, the bending effect in the middle of the fin, which has been repeated in all of snap shots of a-e, is corresponding to the fluid-structure interaction effects. Attention to Fig. 10, which is reported for a case of a stiffer fin (compared to the case of Fig. 9), indicates that the observed bending effect in Fig. 9, which is due to

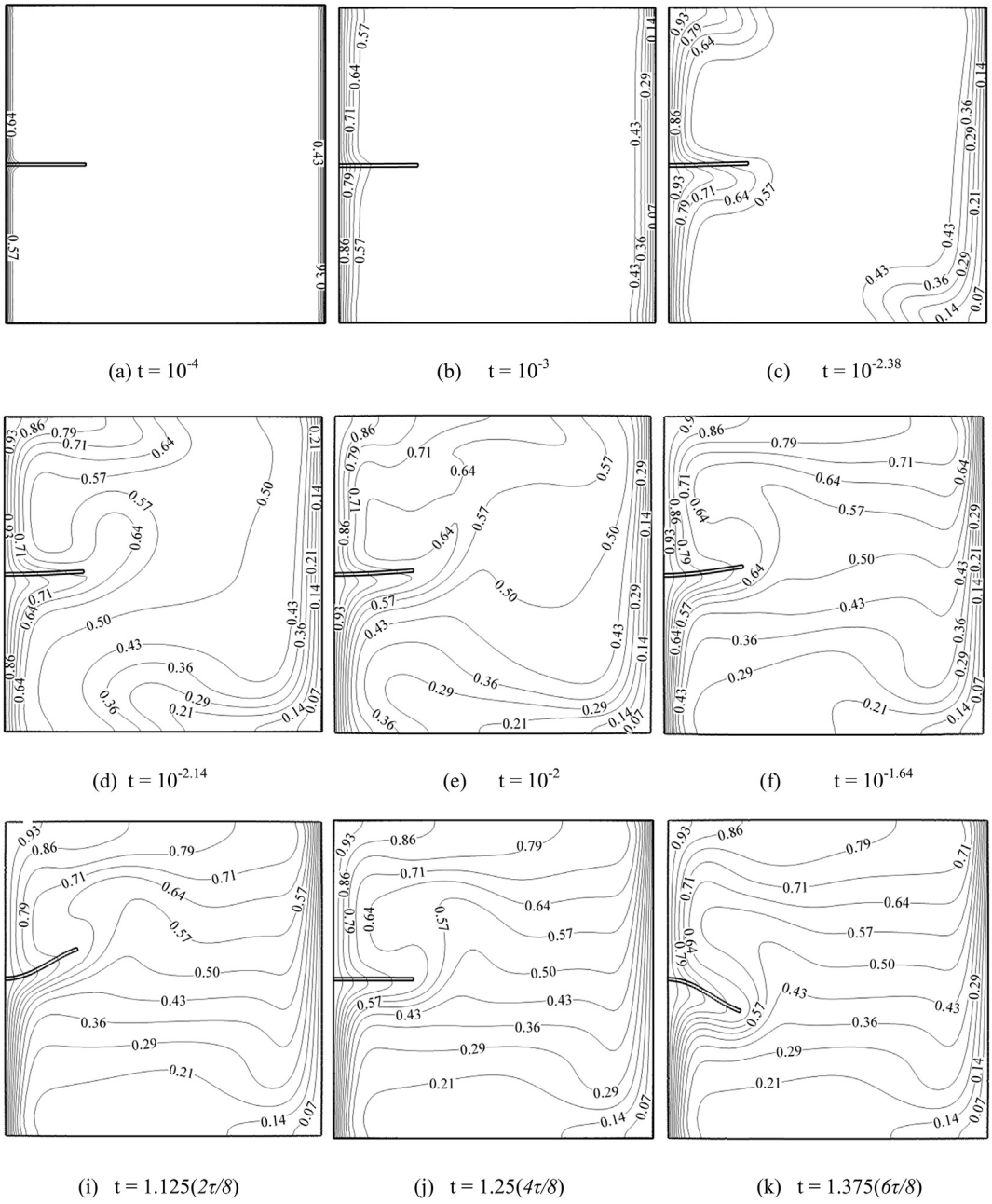

Fig. 8. Isotherms for various dimensionless times at $E = 10^{11}$, $\tau = 0.5$, $A = 0.1$, $k_r = 10$, $Ra = 10^6$, $Pr = 0.7$.

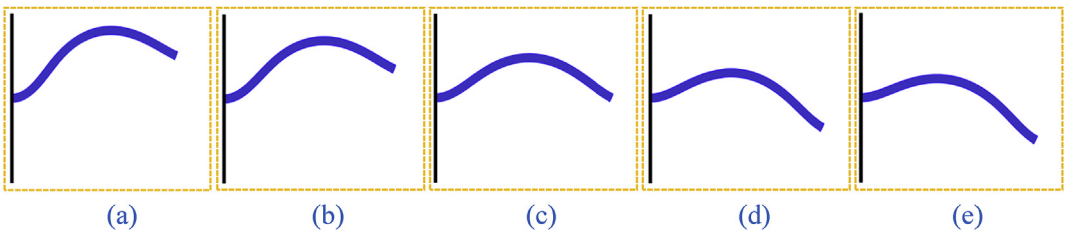

Fig. 9. Fluid-structure interaction between the fluid and the fin when $E = 10^8$.

the fluid-structure effect, is now diminished, and the fin tends to follow the structural behavior of the fin as if there is no fluid involved. In Figs. 11 and 12, the fin completely follows the behavior of a simple cantilever beam subject to a prescribed forced displacement at its tip, and the fluid structure effects can be neglected. Although in Figs. 11 and 12 the shape of the fin is not

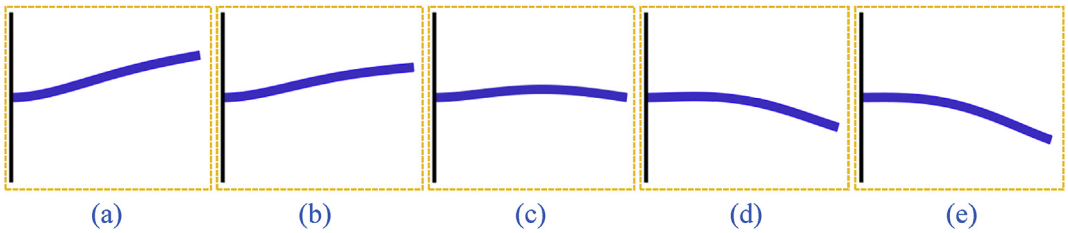

Fig. 10. Fluid-structure interaction between the fluid and the fin when $E = 10^9$.

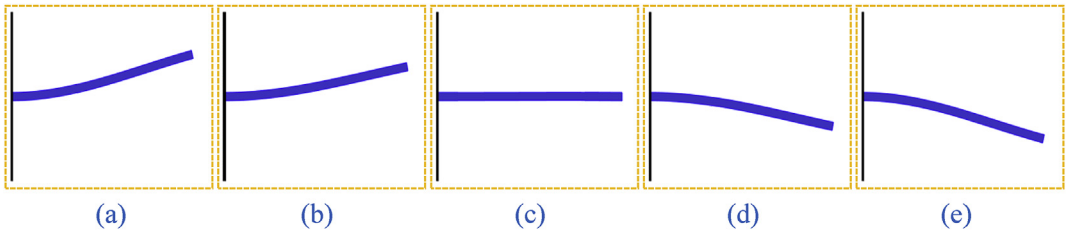

Fig. 11. Fluid-structure interaction between the fluid and the fin when $E = 10^{12}$.

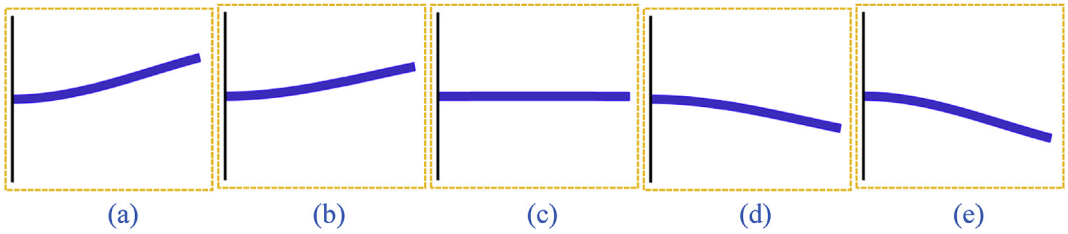

Fig. 12. Fluid-structure interaction between the fluid and the fin when $E = 10^{13}$.

Table 6
The maximum non-dimensional stress in the fin, normalized based on the non-dimensional Young's modulus (σ_{max}/E) when $\tau = 0.1$, $A = 0.05$, $Ra = 10^6$ and $Pr = 0.7$.

t	$E = 10^8$	$E = 10^9$	$E = 10^{12}$	$E = 10^{13}$
(a): $t = 2\tau/8$	3390	367	548.8	548.58
(b): $t = 3\tau/8$	3650	329	298.95	297.81
(c): $t = 4\tau/8$	4790	239	5.37	3.244
(d): $t = 5\tau/8$	6310	1233	299.7	380.99
(e): $t = 6\tau/8$	5770	1540	535.19	543.57

under the influence of the fluid structure interaction, the fluid is under the significant influence of the fin's motion. This effect can be observed by the comparison between the streamlines of Fig. 7 (e) and 7 (j) where the fin reaches its natural straight position. The results of Fig. 7 are reported for $E = 10^{11}$, which is a high non-dimensional Young's modulus, and consequently, the shape of the fin is not under the significant influence of the fluid interaction. In both Fig. 7 (e) and (j), the fin is at its rest position; however, in Fig. 7 (e), the fin moves upward and in Fig. 7 (j), the fin moves downward. A comparison between these two figures indicates a significant difference in the streamlines near the fin, which confirms that the structure motion significantly affects the fluid motion. The same results can be observed for the thermal behavior in the cavity by observing Fig. 8 (e) and (j).

Fig. 13 shows the effect of the non-dimensional Young's modulus (E) on the Nusselt number as a function of the non-dimensional time (t). Fig. 14 shows the non-dimensional heat transfer rate at the basis of the fin for different values of the non-dimensional Young's modulus (E). Fig. 13 shows that, in the case of a very flexible fin ($E = 10^8$), the overall heat transfer (Nu) increments significantly. However, as the stiffness of the fin increases, the heat transfer decreases. Fig. 14 demonstrates that the change in the shape of the flexible fin tends to reduce the heat transfer rate in the basis of the fin. Therefore, it can be concluded that a flexible fin induces a positive influence on the flow and heat transfer of the fluid, in a way to absorb more effectively the heat from the hot wall of the cavity. In the case of a cavity with the same fin but fixed, the

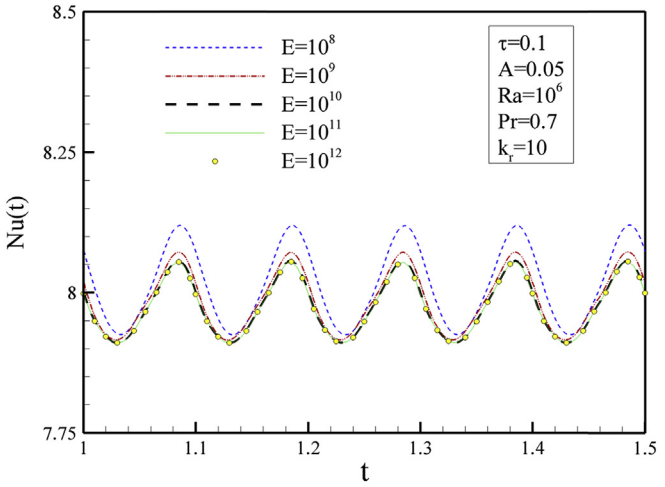

Fig. 13. The influence of the non-dimensional Young's modulus (E) on Nusselt number over dimensionless time.

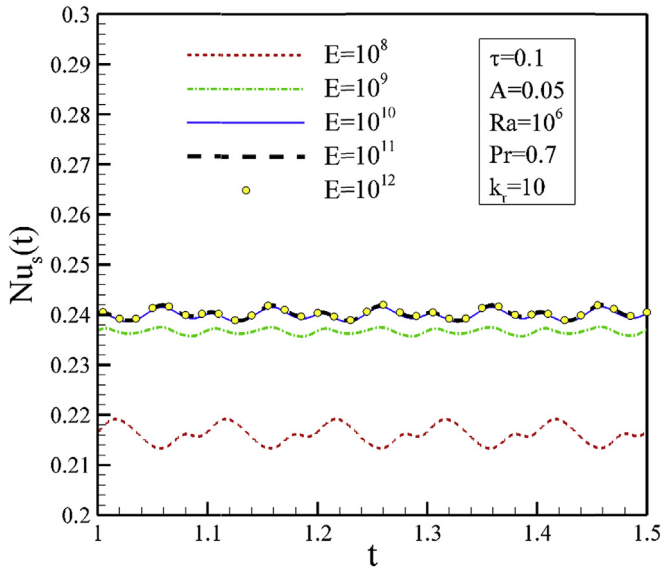

Fig. 14. Influence of Young's modulus on $Nu_s(t)$ as a function of non-dimensional time.

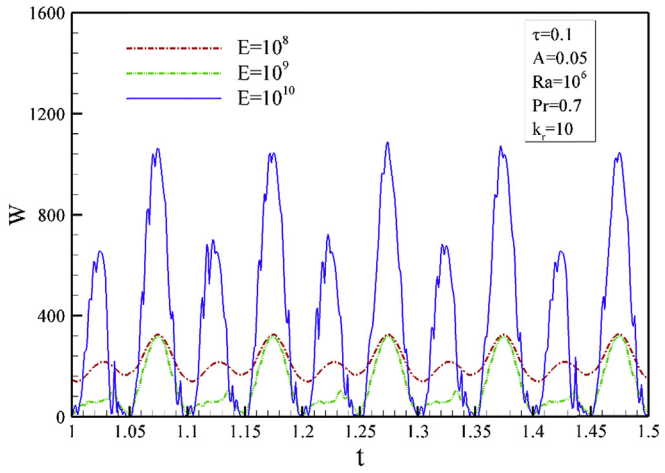

Fig. 15. Time history of the non-dimensional work applied on the fin for various values of the non-dimensional Young's modulus.

steady state average Nusselt number is 7.96. This Nusselt number is below the center line of the oscillation of Nusselt number in Fig. 13, and hence, it can be concluded that the oscillation of the fin enhances the heat transfer in the cavity.

As seen, both Figs. 13 and 14 show that the heat transfer curves for $E = 10^{11}$ and $E = 10^{12}$ are coincident. This result is in agreement with the changes in the shape of the fin which was discussed in Figs. 11 and 12. In fact, in the cases of high values of E, the shape of a stiff fin is not under the influence of the fluid interaction. Hence, when the non-dimensional Young's modulus (E) is high, the increment of E does affect neither the total Nusselt number at the hot wall (Nu (t)) nor the heat transfer rate at the basis of the fin (Nu_s (t)). The ratio of the non-dimensional stress to the non-dimensional Young's modulus (σ/E) shows the normalized stress in the fin. Table 6 is also in agreement with the results of Figs. 9–13 and shows that σ_{max}/E is not under a significant influence of the fluid interaction for high values of E, i.e. $E = 10^{11}$ and $E = 10^{12}$.

Fig. 15 shows the required non-dimensional work for oscillation of the fin for various values of the non-dimensional Young's modulus. The required work for the oscillation of the fin is constructed from two parts, the first one is the mechanical fluid-interaction work which is the result of the fin and the fluid interaction. The second part of the work is the structural mechanical work required for deformation of the solid structure of the fin. The total non-dimensional work performed on the fin is the product of the non-dimensional reaction force on the tip of the fin and the non-dimensional displacement of the fin, as discussed in Eq. (31). The total work is the sum of the mechanical work for deflection of the elastic fin and the work required for interaction with the fluid. Fig. 15 shows that the required work exhibits an oscillatory behavior. As the displacement of the fin tip increases, the fin gets stiffer, and hence, it demands more structural mechanical work. In addition, the increase of the non-dimensional Young's modulus (E) boosts the required structural mechanical work for deflection of the fin. Thus, as seen, the highest work in Fig. 15 corresponds to the case of a very stiff fin, i.e. $E = 10^{10}$. When the stiffness of the fin is low, the work of interaction between the fluid and the structure is important. The comparison between the work history for the two cases of the fins with $E = 10^8$ and $E = 10^9$ reveals that in the case of a very flexible fin of $E = 10^8$, the required total work is higher than that of $E = 10^9$. Indeed, in the case of a fin with $E = 10^8$, the interaction between the fluid and structure is completely significant. Fig 13 confirms that the highest Nusselt number also corresponds to the case of the fin with $E = 10^8$.

Fig. 16 compares the total required work with the structural mechanical part of the work required for oscillation of the fin. The structural mechanical part of the work is evaluated for a fin that moves in a vacuum. The total work is the sum of the structural mechanical and fluid-structure interaction work. It is worth noticing that for a fin oscillating in a vacuum, the fluid-structure part of the total work is zero; however, the structural mechanical part of the work required to oscillatory change the shape of the fin is not zero.

Fig. 16 reveals that for a very flexible fin, i.e. $E = 10^8$, the structural mechanical part of the work is negligible compared to the fluid-structural part of the work required for oscillation of the fin. The same conclusion was derived in the description of Fig. 15. However, as the fin gets stiffer, i.e. $E = 10^9$, the required structural mechanical work for oscillation of the fin increases, but the total work is almost the same. Further increase of the fin's stiffness, i.e. $E = 10^{10}$ and $E = 10^{11}$, the required structural mechanical work significantly boosts and the total work also rises. In Fig. 16 (d), the structural work and the total work are almost coincident. This indicates that the fluid work compared to the required structural mechanical work is negligible. In Fig. 16 (c), the structural mechanical work and the fluid work are almost comparable.

In Fig. 16 (c), the interval of $t = 1$ to $t = 1.05$ corresponds to the time interval in which the fin commences to move upward. Interestingly in this interval, the structural mechanical work is higher than the total work. This is due to the fact that the fluid moves upward, and hence, it helps the fin to move in agreement with the flow direction. However, in the internal of $t = 1.05$ to $t = 1.1$, the fin moves downward which is in disagreement with the upward direction of the natural convective flow, and hence, the total work is significantly higher than that of the structural mechanical work.

4.3. The effect of Rayleigh number

Fig. 17 presents the effect of the Rayleigh number on the streamlines and isotherms at maximum fin tip deflection ($t = 10^{-1}$ corresponding to $t = 2\tau/9$), for $\tau = 0.5$ and $A = 0.1$. For a lower Ra number ($Ra = 10^4$), the streamlines are aligned in a single weak circulation with a stagnant zone localized above the fin. The corresponding isotherms appear to be non-congested (relaxed) with

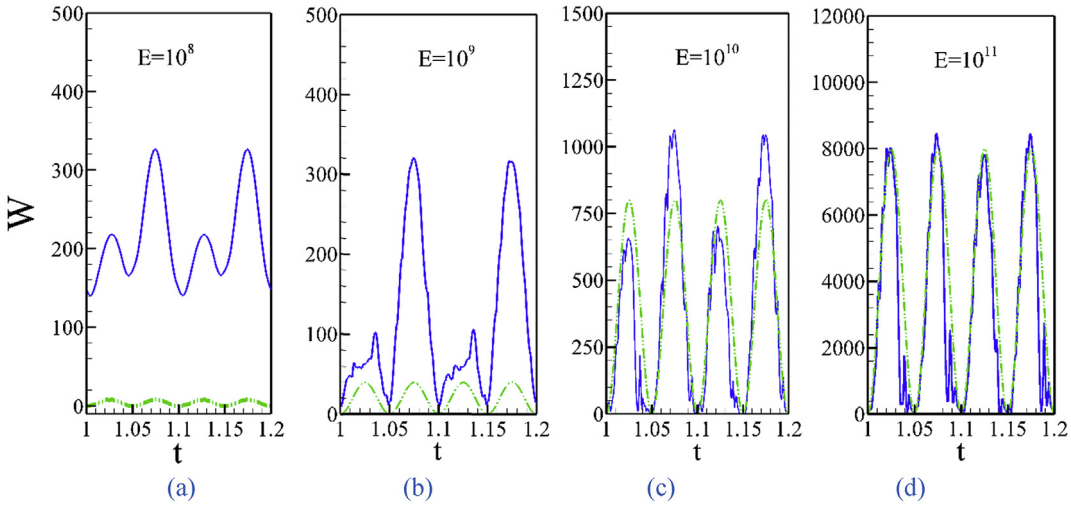

Fig. 16. A comparison between the required structural mechanic work and the total work for oscillation of a fin when $\tau = 0.1$, $A = 0.05$, $Ra = 10^6$ and $Pr = 0.7$: the blue solid curves denote the total work, and the dashed green curves denote the structural mechanical work. (For interpretation of the references to colour in this figure legend, the reader is referred to the web version of this article.)

mostly a vertical pattern, indicating the dominance of conduction. For a higher *Ra* number ($Ra = 10^5$), the buoyancy effect strengthens the streamlines while the stagnant zone above the fin is permeated by the main circulation vortex. Due to the corresponding isotherms, the isotherms close to the left lower (below fin) and the right upper portions of the vertical walls are less crowded. When the *Ra* number is further increased to 10^6 (Fig. 17c), the multicellular behavior of the streamlines is seen and the main vortex breaks up with an intensified flow below the fin surface and close to the right cold wall. This behavior is enhanced when *Ra* is increased to 10^7 (Fig. 17d), where two secondary vortices occupying the left upper zone (above the fin) and strong streamlines with a stratification pattern within the middle cavity are observed. The dominance of natural convection is clearly distinguished by the mostly horizontal isotherms at $Ra = 10^6$-10^7, and the thin thermal boundary layers along the vertical wall (Fig. 17d).

Fig. 18 depicts the steady streamlines and isotherms for the case of a cavity with a fixed fin. A comparison between the results of a cavity with a fixed fin and the results of a cavity with an oscillating fin is possible by comparing the results of Figs. 17 and 18. In the case of a cavity with a low Rayleigh number ($Ra = 10^4$ and $Ra = 10^5$), the motion of the fin solely affects the area next to the fin, and the center and other parts of the cavity are completely unaffected. As the Rayleigh number increases ($Ra = 10^6$ and $Ra = 10^7$), the motion of the fin influences larger areas in the cavity including the regions above the fin. It is interesting to note that the motion of the fin mostly affects the regions above the fin rather than the center of the cavity or below the fin. The reason for this behavior could be the flow direction of the convective flow that is upward, and hence, the effect of the fin motion mostly collects at the higher regions of the cavity which are above the fin.

4.4. The effect of thermal conductivity ratio and non-dimensional fin length

Fig. 19 depicts the instantaneous average Nusselt number along the hot wall for different conductivity ratios at $Ra = 10^6$, $\tau = 0.5$, $L = 0.25$, and $A = 0.1$. Initially, very high Nusselt numbers are recorded (Fig. 19a) which indicates undisturbed thermal boundary layers. Then, a rapid decrease in Nu during the period $10^{-5} \leq t \leq 10^{-2}$ is seen. Then, a periodic state prior to completing one fin tip cycle is seen, where when $t \geq 10^{-1}$ there is no quantitative sharp changes with t. This can be demonstrated by Fig. 19b, where it is a continuous evolution to Fig. 19a, but it starts after two cycles of the fin tip oscillation (where the time of one cycle is $t = 0.5$). A pure periodic state of the Nusselt number is shown in Fig. 19b. The materials mush of the oscillating fin also plays a significant role in convective heat transfer, where the low thermal conductivity fin ($k_r \leq 10$) may act as a baffle and may restrict the heat transfer. Moreover, the oscillation movement of the fin is insignificant at lower thermal conductivity ratios, where, relatively, lower amplitudes are observed when $k_r \leq 10$. On the contrary, for higher thermal conductivity ratios, large amount of heat is transferred by convection and a pronounced effect of the fin oscillation can be demonstrated by the higher amplitude of the Nusselt number for $k_r \geq 100$ (Fig. 19b). Table 7 presents the values of the Nusselt number at the end of the fourth cycle.

Ben-Nakhi and Chamkha [10] have discussed the effect of the length of a fixed fin on the total heat transfer in a cavity. They found that the increase of the length of the fixed fin may enhance the heat transfer due to the enhanced conduction mechanism and in some cases, the reduction of the heat transfer is also possible due to its effect on the suppression of the fluid flow and convective heat transfer. Fig. 20 depicts the effect of the fin length on the oscillation enhancement ratio, NNR, of a flexible fin compared to a fixed fin when the non-dimensional Young's modulus is low $E = 10^8$ (the very flexible fin). This figure illustrates the oscillation enhancement ratio, introduced for the maximum Nusselt number (maximum of Nu (t)), the minimum of the Nusselt number (minimum of Nu (t)) and the average Nusselt number (Nu) when the solution reaches the semi steady state condition and monitored over 5 periods of oscillation, i.e. $t \in [1, 1+5\tau]$.

Fig. 20 shows the enhancement of using a short flexible fin over a fixed fin. This figure also illustrates the smooth increase in the Nusselt number of the oscillating fin over the fixed one by the increase of the non-dimensional fin length. However, when the fin reaches to the non-dimensional length of $L = 0.3$, the time average Nusselt number starts to decrease. Therefore, an optimum fin length can be seen about $L = 0.3$. When the length of the fin increases, the oscillation of the fin induces more disturbance and hence, the heat transfer increases. For high values of the fin length, $L > 0.3$, the fin starts to suppress the natural convective flow, and

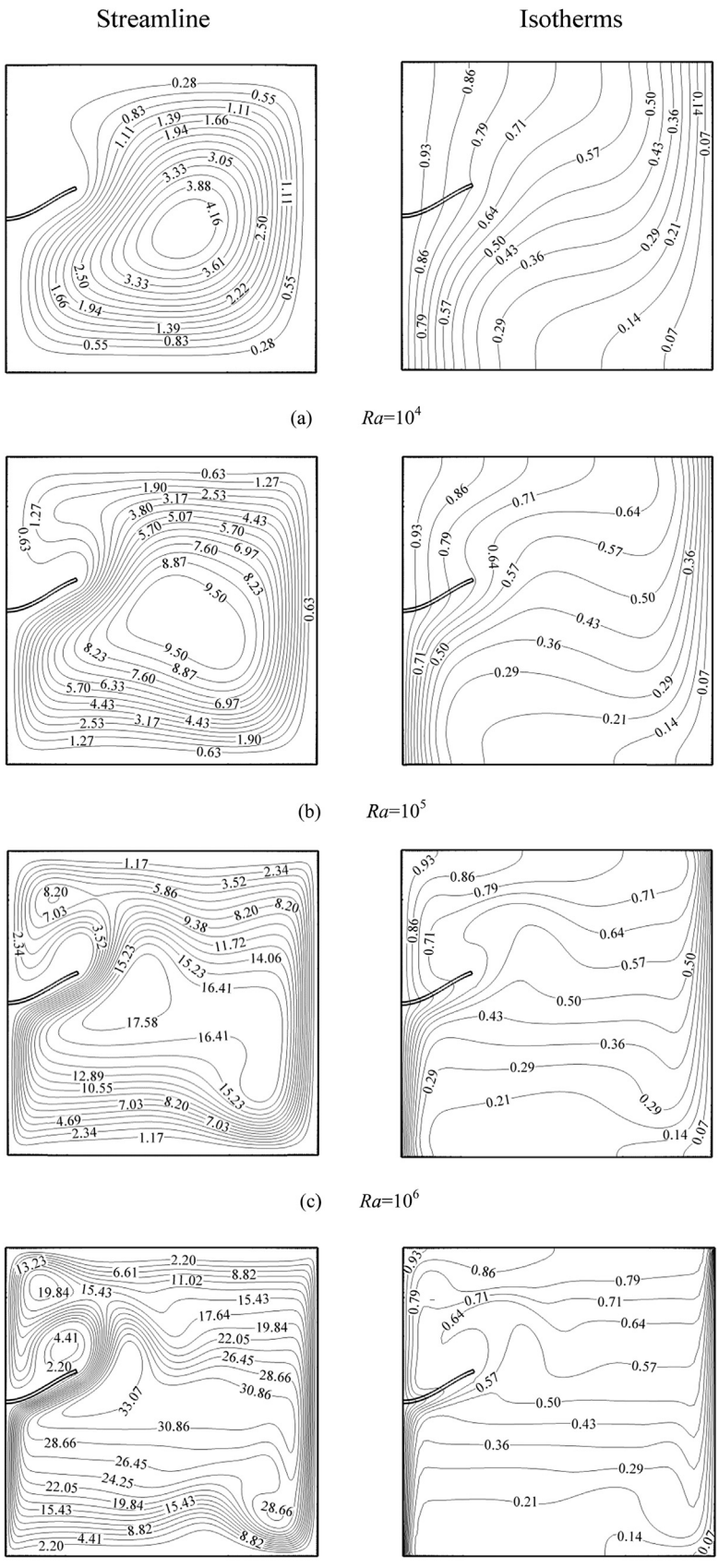

Fig. 17. The isotherms and streamlines for different *Ra* numbers when $E = 10^{11}$, $\tau = 0.5$, $A = 0.1$, $L = 0.25$, $k_r = 10$, $Pr = 0.7$.

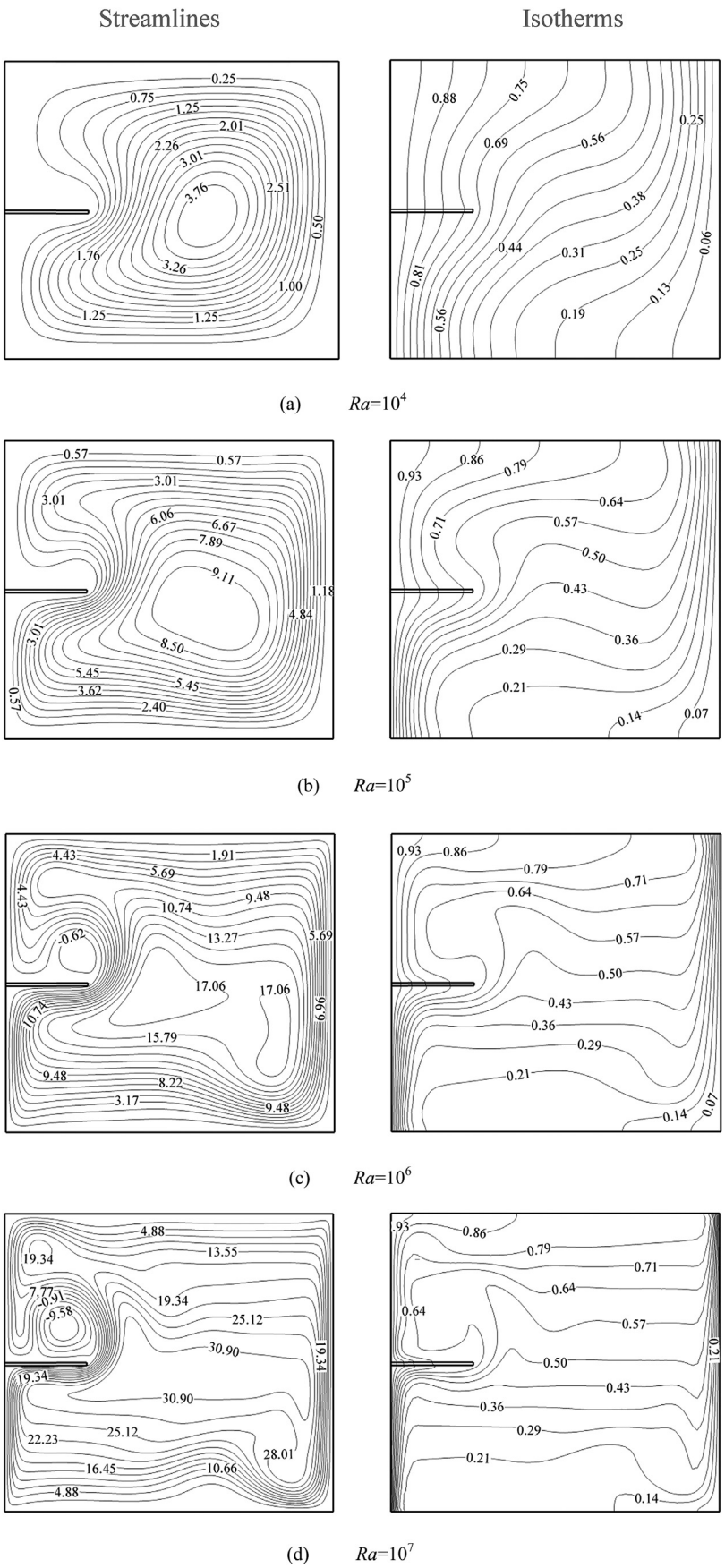

Fig. 18. The isotherms and streamlines for different *Ra* numbers with a fixed the fin at $L = 0.25$, $k_r = 10$, $Pr = 0.7$.

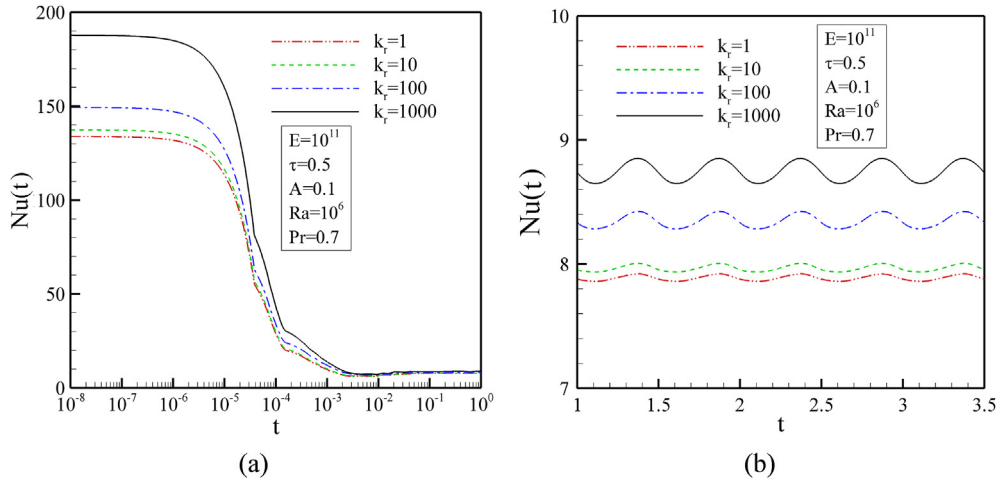

Fig. 19. Variation of Nusselt number with t for different k_r values.

Table 7
Nusselt number with conductivity ratio for $Ra = 10^6$, $\tau = 0.5$, $L = 0.25$, and $A = 0.1$

k_r	Nu
1	7.8890
10	7.9679
100	8.3487
1000	8.7478

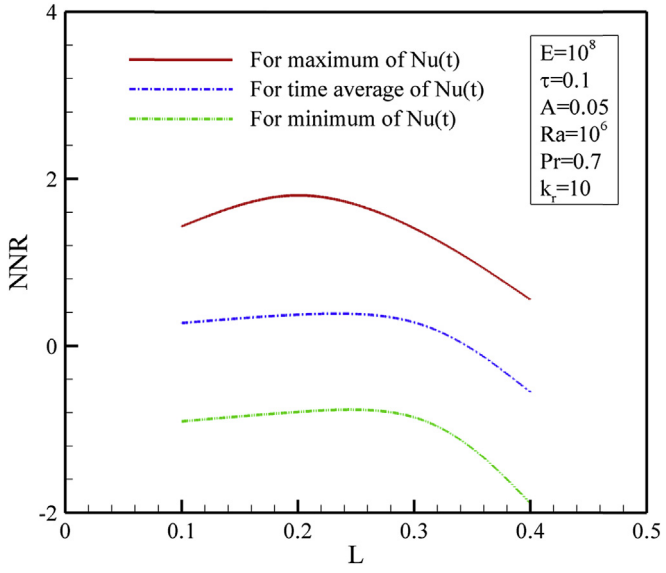

Fig. 20. Effect of the non-dimensional fin length (L) on the enhancement ratio NNR.

the induced disturbance corresponding to the fin oscillation traps below the fin. Hence, for an oscillating fin with a high length, the heat transfer decreases.

4.5. The effect of non-dimensional amplitude and oscillating period

The effect of the non-dimensional fin period (τ) within the periodic state of the Nusselt number is shown in Fig. 21 for $Ra = 10^6$, $L = 0.25$, $A = 0.1$, and $k_r = 10$. The efficient mixing associated with a higher fin tip speed (lower fin period) is the reason behind the noticeably increased Nusselt number amplitude with decreasing values of τ (increasing values of the frequency λ).

Fig. 22 depicts the effect of the fin oscillating amplitude, A, on the Nusselt number for $Ra = 10^6$, $\tau = 0.1$, $L = 0.25$, and $k_r = 10$. Three cycles within the periodic state are shown. It is clear from this figure that the instantaneous Nusselt number is an increasing function of the fin tip amplitude. This is an expected result where at higher amplitudes, larger amount of fluid will be swept resulting in more momentum exchange of the fluid close to the hot wall.

Fig. 23 presents the instantaneous maximum stress (σ) in the fin along two cycles of the periodic state for different fin tip amplitudes A. In this figure, the non-dimensional Young's modulus (E) is high, and hence, the structural mechanical forces are the dominant effects. As expected, the tension in the fin is significantly increased with the increase in the oscillating amplitude. The maximum stress (σ) occurs when the fin reaches its maximum non-dimensional deflection, i.e. $t = \tau/4$ and $t = 3\tau/4$. It is also clear that when the fin reaches its rest position, i.e. $t = 0$, $t = \tau/2$ and $t = \tau$, the maximum stress approaches almost zero.

Fig. 24 is a map containing 121 combinations of τ and A effects on the enhanced ratio of the oscillating fin over the rigid fin (Eq. (30)). This figure depicts that the positive values of NNR which means the enhanced Nusselt number by the oscillating fin over the

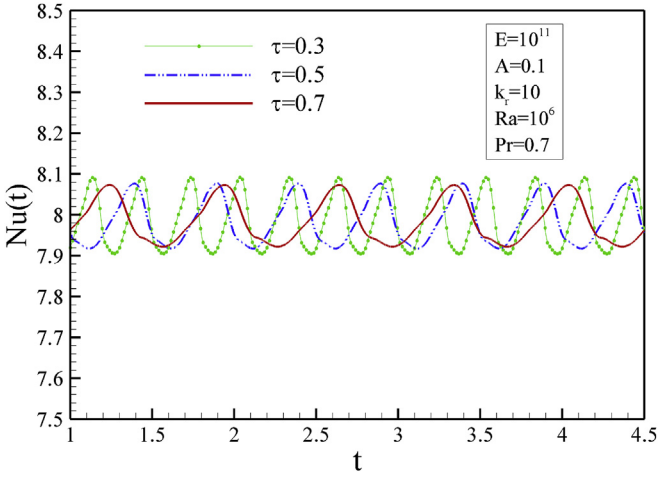

Fig. 21. Effect of non-dimensional fin period τ on the Nusselt number.

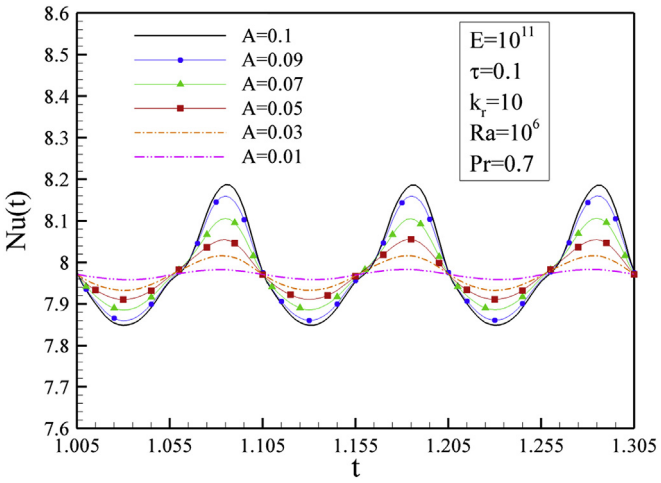

Fig. 22. Effect of the non-dimensional amplitude (A) on the instantaneous Nusselt number during three cycles of fin oscillation.

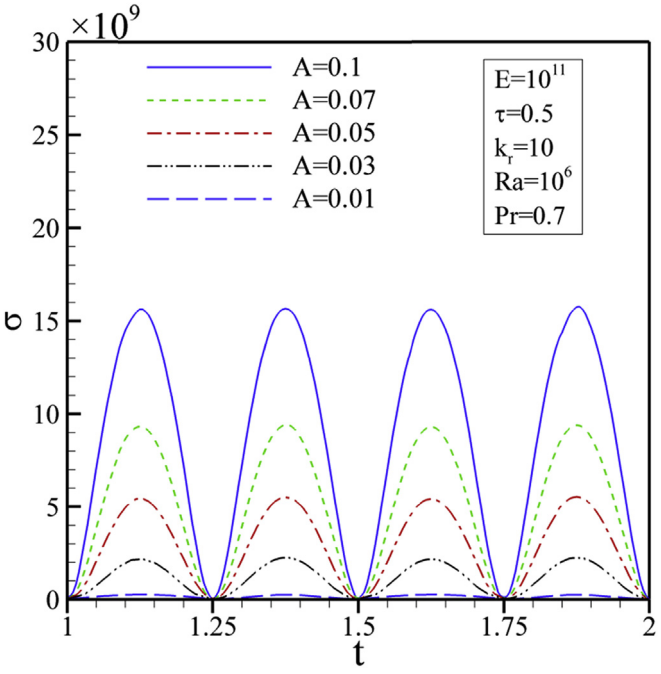

Fig. 23. Maximum non-dimensional stress on the basis of the fin as a function of the non-dimensional time *t*.

rigid fin. It also demonstrates the aforementioned comments that the Nusselt number is an increasing function of the amplitude *A*, but there are optimum periods (τ) for the maximum enhancement ratio, NNR, about $\tau = 0.1$.

5. Conclusions

A fluid structure interaction problem represented by an oscillating elastic fin attached to a hot vertical wall of a square cavity is investigated numerically in the present study. The finite element Galerkin method with the aid of the Arbitrary Lagrangian-Eulerian (ALE) procedure is used. The cavity is differentially heated with the horizontal thermally insulated walls. The elastic fin is assumed to be undergoing an excitation and buoyancy forces. Within the ranges of the aforementioned studied parameters, the following

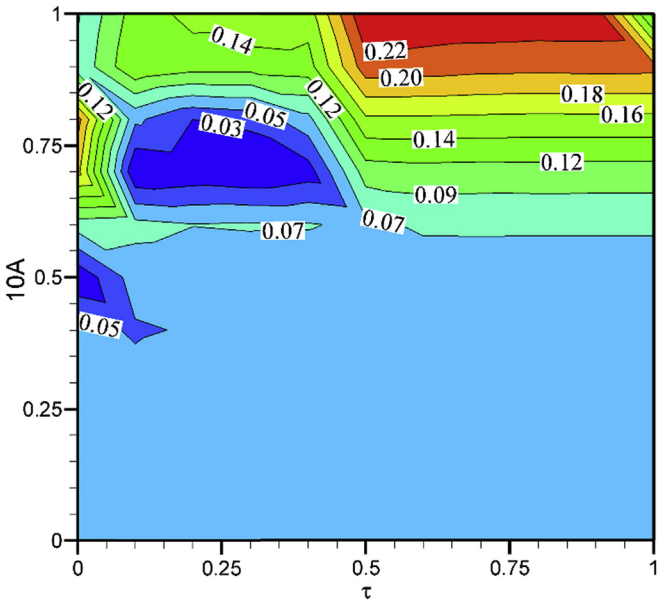

Fig. 24. The patterns of heat transfer improvement (NNR) as a function of fin oscillation periods and amplitude when $E = 10^{11}$, $L = 0.25$, $k_r = 10$.

concluding remarks are drawn from the numerical results.

1 The oscillation of the fin, compared to a fixed fin, mostly enhances the total heat transfer due to its positive effect on the disturbance of the fluid flow next to the hot wall.
2 The required mechanical work for oscillation of the fin is constructed from two parts corresponding to the mechanical fluid-interaction work and the structural mechanical work. The results show that the required total mechanical work for a fin with the non-dimensional Young's modulus of $E = 10^9$ is lower than the cases of $E = 10^8$ and 10^{10}. This is due to the good balance between the required work for the fluid interaction and the required work for the structural mechanical deformation. However, the best heat transfer enhancement is obtained for the case of a very flexible fin, $E = 10^8$. In this case, the required total mechanical work is comparable with the case of minimum required work of $E = 10^9$.
3 The instantaneous average Nusselt number increases with increasing values of the oscillating amplitude. For very low and very high periods of the fin oscillation, the variation of the heat transfer enhancement (NNR) is almost independent of the period. However, about $\tau = 0.1$, there are transient zones in which the increase of the oscillation period enhances the heat transfer.
4 The best utilization of the oscillating fin is when the fin is short. The increase of the length of the oscillating fin smoothly increases the heat transfer enhancement of NNR. However, for fins with high lengths, i.e. $L > 0.3$, the increase of the length of the fin decreases NNR.
5 The maximum stresses in the oscillating fin increases with increasing values of the oscillating amplitude.
6 For any fin deflection, an intensified flow is congested below the fin surface. The intensification is strengthened for upward fin deflection.

In the present study, the oscillation of the fin is due to the strict oscillating displacement at the tip of the fin. Therefore, every movement of the fin requires external work. However, in some parts of the oscillating cycles, when the fin tends to move towards

its resting position due to restoring mechanical structural work, and especially, when the restoring mechanical work and the fluid interaction forces are in agreement, some parts of the work may be restored in a device and then reused in some other parts of the cycle. Moreover, the practical effectiveness of using an oscillating fin depends on the thermal conductivity of the fin and the fluid. On the other hand, the work required for the oscillation of the fin depends on the mechanism, providing the oscillation movement of the fin. In addition, the quality of the mechanical work energy is different with the quality of the thermal energy. Thus, deciding on the thermal effectiveness of using an oscillating fin for heat transfer enhancement or heat and flow control in a cavity requires a detailed entropy analysis, which could be subject of future studies.

Acknowledgements

The first and second authors acknowledge the financial support of Dezful Branch, Islamic Azad University, Dezful. The authors acknowledge the Sheikh Bahaei National High Performance Computing Center (SBNHPCC) for providing computational resources. SBNHPCC is supported by scientific and technological department of presidential office and Isfahan University of Technology (IUT).

References

[1] Fu WS, Shieh WJ. A study of thermal convection in an enclosure induced simultaneously by gravity and vibration. Int J Heat Mass Transf 1992;35(7):1695–710.
[2] Fu WS, Shieh WJ. Transient thermal convection in an enclosure induced simultaneously by gravity and vibration. Int J Heat Mass Transf 1993;36(2):437–52.
[3] Kimoto H, Ishida H. Vibration effects on the average heat transfer characteristics of the natural convection field in a square enclosure. Heat Transfer—Asian Res 2000;29(7):545–58.
[4] Fu WS, Ke WW, Wang KN. Laminar forced convection in a channel with a moving block. Int J Heat Mass Transf 2001;44(13):2385–94.
[5] Florio LA, Harnoy A. Use of a vibrating plate to enhance natural convection cooling of a discrete heat source in a vertical channel. Appl Therm Eng 2007;27(13):2276–93.
[6] Razi YP, Maliwan K, Carrier-Mojitobi MC, Mojitobi A. The influence of mechanical vibrations on buoyancy induced convection in porous media. In: Handbook of porous media; 2005. p. 321–70.
[7] Chung S, Vafai K. Vibration induced mixed convection in an open-ended obstructed cavity. Int J Heat Mass Transf 2010;53(13):2703–14.
[8] Cheng L, Luan T, Du W, Xu M. Heat transfer enhancement by flow-induced vibration in heat exchangers. Int J Heat Mass Transf 2009;52(3):1053–7.
[9] Ben-Nakhi A, Chamkha AJ. Effect of length and inclination of a thin fin on natural convection in a square enclosure. Numer Heat Transf 2006;50(4):381–99.
[10] Ben-Nakhi A, Chamkha AJ. Conjugate natural convection in a square enclosure with inclined thin fin of arbitrary length. Int J Therm Sci 2007;46(5):467–78.
[11] Turek S, Hron J. Proposal for numerical benchmarking of fluid-structure interaction between an elastic object and laminar incompressible flow. Springer Berlin Heidelberg; 2006. p. 371–85.
[12] Vigmostad SC, Udaykumar HS, Lu J, Chandran KB. Fluid–structure interaction methods in biological flows with special emphasis on heart valve dynamics. Int J Numer methods Biomed Eng 2010;26(3–4):435–70.
[13] Dunne T, Rannacher R. Adaptive finite element approximation of fluid-structure interaction based on an Eulerian variational formulation. In: Fluid-structure Interact. Springer Berlin Heidelberg; 2006. p. 110–45.
[14] Heil M, Hazel AL, Boyle J. Solvers for large-displacement fluid–structure interaction problems: segregated versus monolithic approaches. Comput Mech 2008;43(1):91–101.
[15] Bhardwaj R, Mittal R. Benchmarking a coupled immersed-boundary-finite-element solver for large-scale flow-induced deformation. AIAA J 2012;50(7):1638–42.
[16] Tian FB, Dai H, Luo H, Doyle JF, Rousseau B. Fluid–structure interaction involving large deformations: 3D simulations and applications to biological systems. J Comput Phys 2014;258:451–69.
[17] Lee J, You D. Study of vortex-shedding-induced vibration of a flexible splitter plate behind a cylinder. Phys Fluids (1994-present) 2013;25(11):110811.
[18] Khanafer K, Alamiri A, Pop I. Fluid–structure interaction analysis of flow and heat transfer characteristics around a flexible microcantilever in a fluidic cell. Int J Heat Mass Transf 2010;53(9):1646–53.
[19] Soti AK, Bhardwaj R, Sheridan J. Flow-induced deformation of a flexible thin structure as manifestation of heat transfer enhancement. Int J Heat Mass Transf 2015;84:1070–81.
[20] Toda M, Osaka S. Vibrational fan using the piezoelectric polymer PVF 2. Proc IEEE 1979;67(8):1171–3.
[21] Yoo JH, Hong JI, Cao W. Piezoelectric ceramic bimorph coupled to thin metal plate as cooling fan for electronic devices. Sensors Actuators A Phys 2000;79(1):8–12.
[22] Acikalin T, Wait SM, Garimella SV, Raman A. Experimental investigation of the thermal performance of piezoelectric fans. Heat Transf Eng 2004;25(1):4–14.
[23] Liu SF, Huang RT, Sheu WJ, Wang CC. Heat transfer by a piezoelectric fan on a flat surface subject to the influence of horizontal/vertical arrangement. Int J Heat Mass Transf 2009;52(11):2565–70.
[24] Kimber M, Garimella SV. Measurement and prediction of the cooling characteristics of a generalized vibrating piezoelectric fan. Int J Heat Mass Transf 2009;52(19):4470–8.
[25] Ma HK, Li YT. Thermal performance of a dual-sided multiple fans system with a piezoelectric actuator on LEDs. Int Commun Heat Mass Transf 2015;66:40–6.
[26] Sheu WJ, Chen GJ, Wang CC. Performance of piezoelectric fins for heat dissipation. Int J Heat Mass Transf 2015;86:72–7.
[27] Fu WS, Yang SJ. A new model for heat transfer of fins swinging back and forth in a flow. Int J Heat Mass Transf 2001;44(9):1687–97.
[28] Shi X, Khodadadi JM. Fluid flow and heat transfer in a lid-driven cavity due to an oscillating thin fin: transient behavior. J Heat Transf 2004;126(6):924–30.
[29] Shi X, Khodadadi JM. Periodic state of fluid flow and heat transfer in a lid-driven cavity due to an oscillating thin fin. Int J Heat Mass Transf 2005;48(25):5323–37.
[30] Jamesahar E, Ghalambaz M, Chamkha AJ. Fluid–solid interaction in natural convection heat transfer in a square cavity with a perfectly thermal-conductive flexible diagonal partition. Int J Heat Mass Transf 2016;100:303–19.
[31] Hirt CW, Amsden AA, Cook JL. An arbitrary Lagrangian-Eulerian computing method for all flow speeds. J Comput Phys 1974;14(3):227–53.
[32] Hughes TJ, Liu WK, Zimmermann TK. Lagrangian-Eulerian finite element formulation for incompressible viscous flows. Comput methods Appl Mech Eng 1981;29(3):329–49.
[33] Donea J, Giuliani S, Halleux JP. An arbitrary Lagrangian-Eulerian finite element method for transient dynamic fluid-structure interactions. Comput methods Appl Mech Eng 1982;33(1–3):689–723.
[34] Kuhl E, Hulshoff S, De Borst R. An arbitrary Lagrangian Eulerian finite-element approach for fluid–structure interaction phenomena. Int J Numer methods Eng 2003;57(1):117–42.
[35] Donea J, Huerta A. Finite element methods for flow problems. John Wiley & Sons; 2003.
[36] Deng QH, Tang GF. Numerical visualization of mass and heat transport for conjugate natural convection/heat conduction by streamline and heatline. Int J Heat Mass Transf 2002;45(11):2373–85.
[37] Anandalakshmi R, Basak T. Heat flow visualization for natural convection in rhombic enclosures due to isothermal and non-isothermal heating at the bottom wall. Int J Heat Mass Transf 2012;55(4):1325–42.
[38] de Vahl Davis G. Natural convection of air in a square cavity: a bench mark numerical solution. Int J Numer methods fluids 1983;3(3):249–64.
[39] Shi X, Khodadadi JM. Laminar natural convection heat transfer in a differentially heated square cavity due to a thin fin on the hot wall. J Heat Transf 2003;125(4):624–34.
[40] Sathiyamoorthy M, Chamkha J. Analysis of natural convection in a square cavity with a thin partition for linearly heated side walls. Int J Numer Methods Heat Fluid Flow 2014;24(5):1057–72.
[41] Nag A, Sarkar A, Sastri VMK. Natural convection in a differentially heated square cavity with a horizontal partition plate on the hot wall. Comput methods Appl Mech Eng 1993;110(1):143–56.
[42] Kaminski DA, Prakash C. Conjugate natural convection in a square enclosure: effect of conduction in one of the vertical walls. Int J Heat Mass Transf 1986;29(12):1979–88.
[43] Ben-Nakhi A, Chamkha AJ. Conjugate natural convection in a square enclosure with inclined thin fin of arbitrary length. Int J Therm Sci 2007;46(5):467–78.
[44] Xu F, Patterson JC, Lei C. Heat transfer through coupled thermal boundary layers induced by a suddenly generated temperature difference. Int J Heat Mass Transf 2009;52(21):4966–75.